

A crucial role for the cortical amygdala in shaping social encounters

<https://doi.org/10.1038/s41586-024-08540-4>

Received: 2 June 2023

Accepted: 17 December 2024

Published online: 12 February 2025

Open access

 Check for updates

Antonio V. Aubry^{1,2,3,14}, Romain Durand-de Cuttoli^{1,2,3,14}, Elizabeth Karpman^{1,2,3}, Rachel L. Fisher-Foye^{1,2,3}, Lyonna F. Parise^{1,2,3}, Flurin Cathomas^{1,2,3}, C. Joseph Burnett^{1,2,3}, Yewon Yang^{1,2,3}, Chongzhen Yuan^{4,5}, Alexa R. LaBanca^{1,2,3}, Kenny L. Chan^{1,2,3}, Kion T. Winston^{1,2,3}, Hsiao-yun Lin^{1,2,3}, Farah Dackour^{1,2,3}, Arman A. Tavallaei^{1,2,3}, Johana Alvarez^{1,2,3}, Tadaaki Nishioka^{1,6,7}, Hirofumi Morishita^{1,6,7,8,9}, Robert C. Froemke^{10,11,12,13}, Long Li^{4,5}✉ & Scott J. Russo^{1,2,3}✉

Aggression is an evolutionarily conserved behaviour that controls social hierarchies and protects valuable resources. In mice, aggressive behaviour can be broken down into an appetitive phase, which involves approach and investigation, and a consummatory phase, which involves biting, kicking and wrestling¹. Here, by performing an unsupervised weighted correlation network analysis on whole-brain FOS expression in mice, we identify a cluster of brain regions, including hypothalamic and amygdalar subregions and olfactory cortical regions, that are highly co-activated in male but not in female aggressors. The posterolateral cortical amygdala (COApI)—an extended olfactory structure—was found to be a hub region, on the basis of the number and strength of correlations with other regions in the cluster. Our data also show that oestrogen receptor 1 (*Esr1*)-expressing cells in the COApI (COApI^{Esr1}) exhibit increased activity during attack behaviour and during bouts of investigation that precede an attack, in male mice only. Chemogenetic or optogenetic inhibition of COApI^{Esr1} cells in male aggressors reduces aggression and increases pro-social investigation without affecting social reward and reinforcement behaviour. We further show that COApI^{Esr1} projections to the ventromedial hypothalamus and central amygdala are necessary for these behaviours. Collectively, these data suggest that, in aggressive males, COApI^{Esr1} cells respond specifically to social stimuli, thereby enhancing their salience and promoting attack behaviour.

Aggressive behaviours are complex forms of social behaviour that have many functions, including acquiring resources to help ensure survival. These behaviours are composed of an appetitive and consummatory phase¹. In mice, the appetitive phase involves approach and investigation, whereas the consummatory phase involves a series of motor behaviours such as biting, kicking or wrestling^{2,3}. Our laboratory has previously characterized a population of outbred mice that exhibit individual differences in aggressive and pro-social behaviour in the resident-intruder (RI) test, allowing us to evaluate the underlying neural mechanisms^{3–7}. Although studies have identified several brain regions in the hypothalamus and ventral striatum that enable aggressive behaviour^{4,6,8–10}, little work has been done to identify the brain regions that have a role in the transition between appetitive and consummatory phases of aggressive behaviours. Understanding the mechanisms of this transition is crucial, because it is one of the processes that distinguishes

aggressive mice (AGGs) from non-aggressive mice (NONs). Sensory processing has been shown to be key in the transition between these phases during other social behaviours such as parenting and social recognition^{11,12}. However, whether activity in sensory-processing cortical regions drives differences in aggressive social behaviour is unknown.

We first used an iDISCO+ clearing procedure followed by whole-brain immunostaining to identify FOS⁺ cells. We then used an unsupervised whole-brain computational approach¹³ to identify a cluster of hypothalamic, amygdalar and olfactory cortical regions that are highly co-activated in male but not in female AGGs. Within this cluster, we found that the posterolateral cortical amygdala (COApI), which is part of the olfactory cortex, is a key node or ‘hub region’ that is highly connected within the broader network of this cluster. We further investigated the mechanisms by which the COApI mediates aggressive social behaviour using a variety of circuit techniques. We found

¹Nash Family Department of Neuroscience, Icahn School of Medicine at Mount Sinai, New York, New York, USA. ²Brain and Body Research Center and Friedman Brain Institute, Icahn School of Medicine at Mount Sinai, New York, New York, USA. ³Friedman Brain Institute, Icahn School of Medicine, Mt Sinai, New York, NY, USA. ⁴State Key Laboratory of Cognitive Science and Mental Health, Institute of Biophysics, Chinese Academy of Sciences, Beijing, China. ⁵University of the Chinese Academy of Sciences, Beijing, China. ⁶Department of Psychiatry, Icahn School of Medicine at Mount Sinai, New York, New York, USA. ⁷Mindich Child Health and Development Institute, Icahn School of Medicine, New York, NY, USA. ⁸Department of Ophthalmology, Icahn School of Medicine at Mount Sinai, New York, New York, USA. ⁹Department of Mental Disorder Research, National Institute of Neuroscience, National Center of Neurology and Psychiatry, Tokyo, Japan. ¹⁰Skirball Institute for Biomolecular Medicine, New York University Grossman School of Medicine, New York, NY, USA. ¹¹Department of Neuroscience and Physiology, New York University Grossman School of Medicine, New York, NY, USA. ¹²Neuroscience Institute, New York University Grossman School of Medicine, New York, NY, USA. ¹³Department of Otolaryngology, New York University Grossman School of Medicine, New York, NY, USA. ¹⁴These authors contributed equally: Antonio V. Aubry, Romain Durand-de Cuttoli. ✉e-mail: longli@ibp.ac.cn; scott.russo@mssm.edu

that COAp^{Esr1} neurons, and downstream connections such as the ventromedial hypothalamus (VMH) and the central amygdala (CEA), are highly co-activated during bouts of social investigation that precede an attack, and that these circuits regulate the transition from the appetitive phase (approach and investigation) of aggressive interactions to the consummatory phase (attack).

The COApI is a key node in a male AGG network

After a RI test, we performed a cleared whole-brain FOS mapping experiment using the iDISCO+ method combined with a network analysis that is commonly used in RNA-sequencing studies to identify differentially activated regions between male and female AGGs and NONs (Fig. 1a). Before brain collection, male and female AGGs and NONs were exposed to an intruder mouse. We did not see a difference in total attack duration or investigation duration between the sexes (Fig. 1b,c), but we did observe that males and females engaged in distinct actions that made up the total duration metrics, as previously reported³ (Extended Data Fig. 1a–f). We then assembled a network for both AGGs and NONs (Fig. 1d). After constructing each network, we performed a module preservation analysis using the AGG network as the reference network and the NON network as the test network. We found that the ‘pink’ module was the least preserved module in the NON network (Fig. 1e, Extended Data Fig. 2a–c and Supplementary Data 1). Inspection of this module showed that subregions of the amygdala and hypothalamus are highly interconnected in the AGG network. In the NON network, however, subregions of the hypothalamus and amygdala are highly connected amongst themselves, but not between the amygdala and hypothalamus. Notably, male AGGs expressed this module, as determined by the eigenvalues, significantly more than female AGGs did (Fig. 1f). We also found that many of the top regions that showed a significant increase in FOS counts were different between male and female AGGs (Extended Data Fig. 2e,f). When using the NON network as a reference, we found that the ‘blue’ network, which was composed mainly of regions from the isocortex, was not preserved in the AGGs (Extended Data Fig. 3a). We also constructed a network of AGGs and NONs in response to a novel object. Only two regions from the pink module in male AGGs showed an increase in FOS relative to NONs (the dorsomedial hypothalamus and the subparaventricular zone; Extended Data Fig. 3b). In addition, we ran a preservation analysis comparing the pink module of AGGs and NONs in response to an intruder and in response to a novel object, and found that the pink module was not preserved in response to the novel object in either AGGs or NONs (Extended Data Fig. 3c,d). Of the 28 regions in the pink module (Supplementary Data 2), 11 regions differed in their total connectivity within the pink module between AGGs and NONs. Of the four regions that showed higher connectivity in the AGG network, the posterior cortical amygdala (COAp) had the highest average connectivity (Fig. 1g). Of note, the COAp showed stronger connectivity with the VMH in the AGG network than it did in the NON network.

To further confirm predictions from the network analysis, we recorded local field potentials (LFPs) in the COAp and VMH in awake, behaving mice during the RI test. We found that there was an increase in coherence between the COAp and the VMH during attack behaviour (Fig. 1h,i and Extended Data Fig. 4), but not during isolated bouts of investigation. In-depth analysis revealed that the increase in coherence was in the delta (1.5–4 Hz), theta (5–12 Hz) and gamma (40–100 Hz) bands (Fig. 1i). Further investigation of the COAp showed that male AGGs had more FOS⁺ cells in this region, compared with female AGGs and male NONs in the iDISCO+ dataset (Fig. 1j). Because ClearMap cannot distinguish between the lateral and the medial cortical amygdala, we manually analysed the lateral and the medial portions of the COAp, and found that male AGGs showed a significant increase in the number of cells expressing FOS in the lateral relative to the medial portion (Extended Data Fig. 5a). In the COApI, we found that male AGGs showed a significant increase in the proportion of *Esr1* cells that expressed FOS, relative to female AGGs and

male NONs (Fig. 1k–l). Detailed analyses of this cell population determined that most COApI^{Esr1} cells were glutamatergic (around 90%) and were equally expressed in the COApI in all four groups (Extended Data Fig. 5b–d). We also found that most of the cells that expressed FOS also expressed *Esr1* (around 85%; Extended Data Fig. 5e).

To investigate the activity of COApI^{Esr1} neurons in vivo during aggressive encounters with an intruder mouse, we injected a Cre-dependent adeno-associated virus (AAV) expressing GCaMP6s (AAV-DIO-GCaMP6s) into the COApI of *Esr1*-Cre transgenic mice to label COApI^{Esr1+} neurons (Fig. 2a). We then measured fluorescent Ca²⁺ activity by fibre photometry across three days of the RI test in male and female AGGs. Because the COApI receives input from the main olfactory bulb, we first examined the response of COApI^{Esr1} neurons to six different odours (social (male, female and juvenile male), non-social (peanut scent, object) and predator (fox urine) scents). We found that COApI^{Esr1} neurons exhibited a significant increase in Ca²⁺ activity when mice investigated soiled bedding from a cage of male or female C57 mice, but not when they investigated the other odours (Fig. 2b,c). We also analysed the post-pre response to all six odours by generating a z-score that reflects a change from baseline, and found that the response to adult male odours was significantly higher than the response to all other odours, except juvenile males, which was trending but did not reach statistical significance (Extended Data Fig. 6a). Because previous work has shown that the COApI regulates aversive and appetitive responses to fox urine and peanut odour¹⁴, we performed RNAscope in odorant-naive mice and mice exposed to male bedding, peanut odour and fox urine. We confirmed that all odours elicited an increase in FOS in the COApI relative to naive mice (Extended Data Fig. 6b). However, when we restricted our analysis of FOS to COApI^{Esr1} cells, we found that only bedding elicited a significant increase in FOS relative to naive mice (Extended Data Fig. 6c,d). No significant changes in COApI^{Esr1} FOS were observed in response to peanut odour and predator scent. By contrast, we found that the peanut odour and fox urine elicited a significant increase in FOS cells that did not express *Esr1*. We observed complementary results in female mice, with a significant increase in Ca²⁺ activity during the investigation of soiled bedding from a cage of same-sex mice (Extended Data Fig. 6e), but not during the investigation of fox urine or an ethanol swab (Extended Data Fig. 7f,g).

During the RI test, we observed that COApI^{Esr1} neurons exhibited a significant increase in Ca²⁺ activity during bouts of investigation in trials where an attack occurred, relative to bouts of investigation during trials in which no attack occurred (Fig. 2d,e). By contrast, we observed the opposite effect in females: COApI^{Esr1} neurons showed a significant increase in Ca²⁺ activity during investigation trials in which no attack occurred (Extended Data Fig. 6h). When examining individual investigation bouts during trials in which an attack occurred, we found that COApI^{Esr1} neurons increased Ca²⁺ activity only during bouts of investigation that preceded an attack, compared with bouts of investigation that occurred in isolation (Fig. 2f,g). In females, we did not detect any differences in Ca²⁺ activity in female AGGs between the two types of investigation (Extended Data Fig. 6i). Finally, when examining attack bouts, we found that when attacks were preceded by a bout of investigation, there was no further increase in Ca²⁺ activity during the attack. When an attack occurred spontaneously without prior investigation, we found that there was a significant increase in Ca²⁺ activity during the attack in male (Fig. 2h,i) but not in female (Extended Data Fig. 6j) AGGs. In a separate cohort, we recorded Ca²⁺ activity during social encounters across the four phases of the oestrous cycle, but did not observe any differences in the signal during attack or investigatory behaviours as a function of cycle stage (Extended Data Fig. 6k–m).

Manipulating COApI^{Esr1} cells alters consummatory drive

The results discussed above suggest that COApI^{Esr1} neurons are highly active during the transition from the appetitive phase (approach and

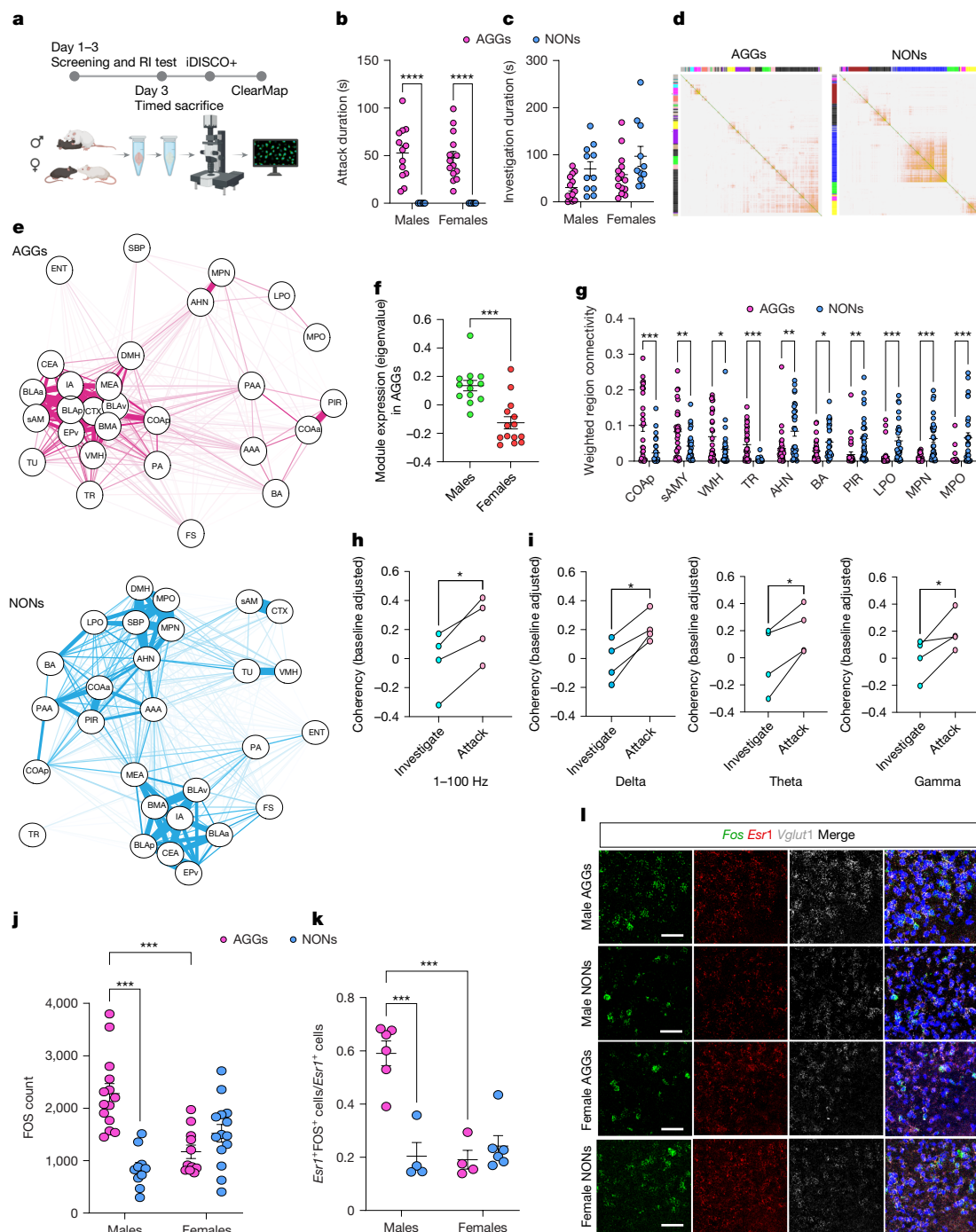


Fig. 1 | The COAp is a key node in a differentially connected module in aggressive males. **a**, Experimental timeline. **b, c**, Aggression duration was significantly higher in AGGs than in NONs (**b**; main effect of phenotype, $F_{(1,44)} = 83.30, P < 0.0001$) and NONs exhibited more social investigation than did AGGs (**c**; main effect of phenotype, $F_{(1,46)} = 6.984, P = 0.0112$) ($n = 13$ male AGGs, 14 female AGGs, 10 male NONs and 13 female NONs). **d**, Whole-brain FOS network analysis in AGGs and NONs. **e**, Network plot of the pink module in AGGs (top) and NONs (bottom). **f**, Male AGGs exhibited higher pink-module expression than did female AGGs ($t_{(25)} = 4.612, P = 0.0001$). **g**, Regions in the pink module differed in intramodular connectivity between AGG and NON networks. All q values were less than 0.05. **h**, Coherency analysis in the COAp–VMH circuit during attack and investigation bouts ($t_3 = 5.412, P = 0.0124$). **i**, Quantification of coherence in the delta ($t_3 = 3.915, P = 0.0296$), theta ($t_3 = 3.904, P = 0.0298$) and gamma ($t_3 = 3.241, P = 0.0478$) bands. **j–l**, FOS expression in the COAp. **j, k**, iDISCO+ revealed a significant phenotype \times sex interaction ($F_{(1,46)} = 24.11, P < 0.0001$), with male AGGs exhibiting higher FOS expression than male NONs ($P < 0.0001$, Tukey’s post-hoc) and female AGGs ($P < 0.0001$, Tukey’s post-hoc). **l**, Fluorescence in situ

hybridization (FISH) revealed that male AGGs also exhibited a higher number of FOS⁺ cells expressing *Esr1* (phenotype \times sex interaction: $F_{(1,16)} = 23.09, P = 0.0002$) than did male NONs ($P < 0.0001$, Tukey’s post-hoc) and female AGGs ($P < 0.0001$, Tukey’s post-hoc) ($n = 6$ male AGGs, 4 female AGGs, 4 male NONs and 6 female NONs). * $P < 0.05$, ** $P < 0.01$, *** $P < 0.001$, **** $P < 0.0001$. All data are mean \pm s.e.m. All network data and corresponding behaviour were replicated in two cohorts. FISH and in vivo electrophysiology were carried out in a single cohort. ENTmv, entorhinal cortex medial part ventral zone; SBPV, subparaventricular zone; MPN, medial preoptic nucleus; AHN, anterior hypothalamic nucleus; LPO, lateral preoptic area; MPO, medial preoptic area; AAA, anterior amygdala area; BA, bed nucleus of anterior commissure; FS, fundus of striatum; PA, posterior amygdala; TR, transition area; TU, tuberal nucleus; EPv, ventral endopiriform area; BMA, basomedial amygdala; CTX, cortical subplate; sAMY, striatal amygdala; BLAa, anterior basolateral amygdala; BLAp, posterior basolateral amygdala; IA, intercalated amygdala; DMH, dorsomedial hypothalamus. The illustrations in **a** were created with BioRender.

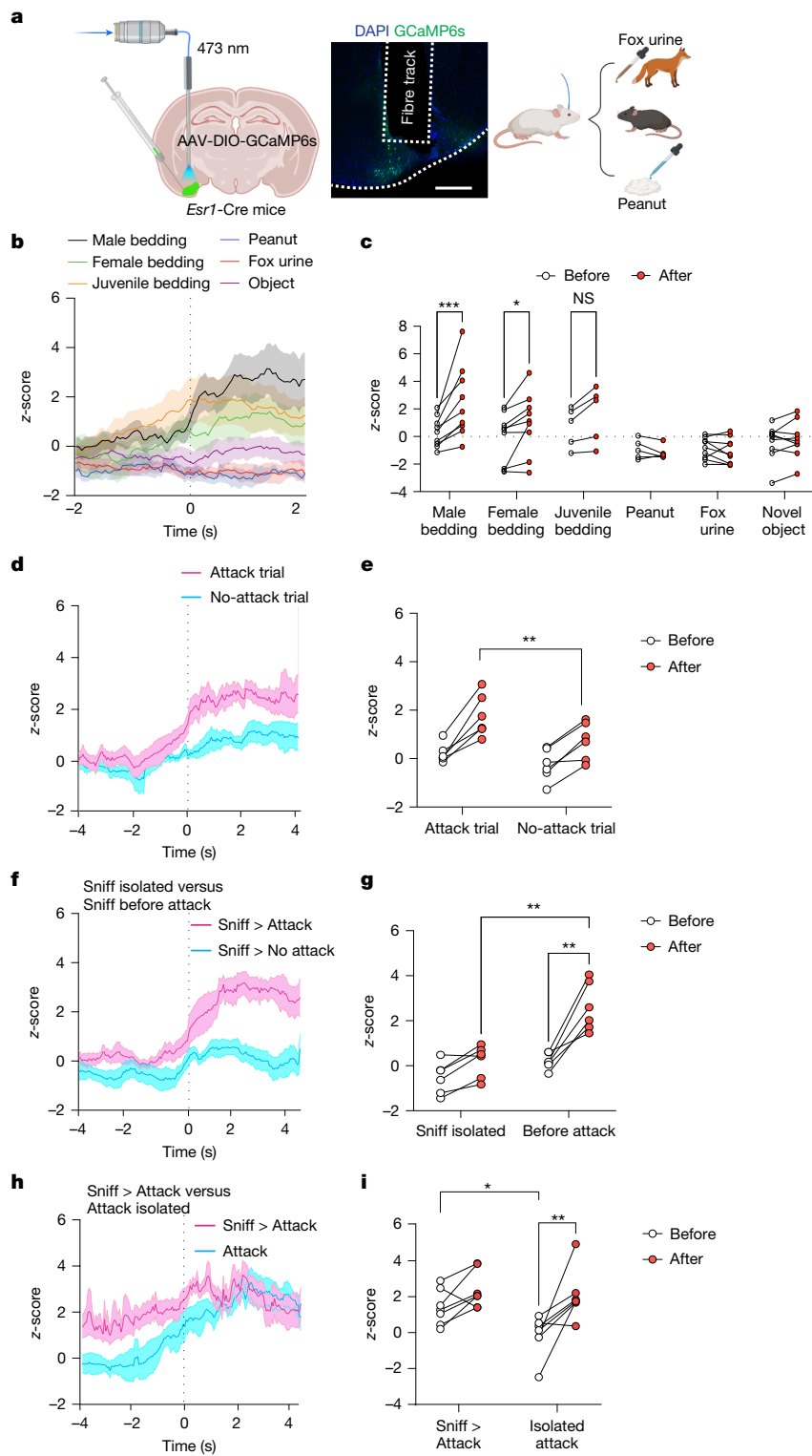


Fig. 2 | In vivo activity of COAp^{Esr1} cells during distinct bouts of investigation in male AGGs. **a**, Experimental timeline. **b**, COAp^{Esr1} activity before and after the investigation of an odour. **c**, There was a main effect of cue ($F_{(5,40)} = 3.689, P = 0.0077$), time ($F_{(1,8)} = 10.89, P = 0.0108$) and a cue \times time interaction ($F_{(5,24)} = 7.716, P = 0.0002$). Post-hoc comparisons revealed an increase in COAp^{Esr1} activity during the investigation of soiled male ($P < 0.0001$) and female ($P = 0.0169$) bedding ($n = 9$ male bedding, $n = 9$ female bedding, $n = 5$ peanut, $n = 5$ juvenile, $n = 9$ fox urine, $n = 9$ object). NS, not significant. **d–i**, COAp^{Esr1} activity before and after social behaviour. **d, e**, There was a significant increase in activity during investigation on an attack day (trial \times time interaction: $F_{(1,5)} = 44.52, P = 0.0011$; **d**) compared with investigation bouts during a no-attack day ($P = 0.0002$, Tukey's post-hoc test; **e**). **f, g**, There was a significant increase in COAp^{Esr1} activity during investigation bouts that preceded an attack (behaviour \times time interaction: $F_{(1,5)} = 9.054, P = 0.0298$; **f**) compared with those that occurred in isolation ($P = 0.0063$, Tukey's post-hoc ($n = 6$); **g**). **h, i**, There was a significant difference in COAp^{Esr1} activity before the onset of attack when mice were engaged in investigation before the attack (behaviour \times time interaction: $F_{(1,6)} = 8.662, P = 0.0258$; **h**) compared with when they were not investigating ($P = 0.0175$, Tukey's post-hoc; **i**). No difference was observed in COAp^{Esr1} activity during attack, regardless of whether it was preceded by a bout of investigation ($P = 0.9989$, Tukey's post-hoc) ($n = 7$). * $P < 0.05$, ** $P < 0.01$, *** $P < 0.001$. All data are mean \pm s.e.m. Scale bar, 200 μ m. Data from this figure were replicated in two cohorts. The illustrations in **a** were created with BioRender.

investigate) of aggressive social interactions to the consummatory phase. To test the hypothesis that this cell population mediates this transition, we first used viral vectors expressing designer receptors exclusively activated by designer drugs (DREADDs) to bidirectionally manipulate the activity of COAp^{Esr1} neurons. Around three to four weeks before the RI and social self-administration tests, we injected AAV-DIO-hM3Dq, AAV-DIO-hM4Di or AAV-DIO-mCherry viruses into the COApI of eight-week-old *Esr1-Cre* mice (Fig. 3a,b). We found that inhibiting COAp^{Esr1} neurons led to a marked reduction in total attack

duration and a concomitant increase in total investigation. Conversely, we found that exciting COAp^{Esr1} neurons led to a significant increase in total attack duration without a decrease in total investigation (Fig. 3c,d). We also injected AAV-DIO-hM4Di into the medial portion of the COAp and did not see any changes in attack behaviour (Extended Data Fig. 7j–l), which is consistent with a previous lesion study in rats¹⁵. When examining distinct aggressive actions, we found that the number of bites during RI was affected most by the inhibition or excitation of COAp^{Esr1} neurons (Extended Data Fig. 7a–c). Furthermore,

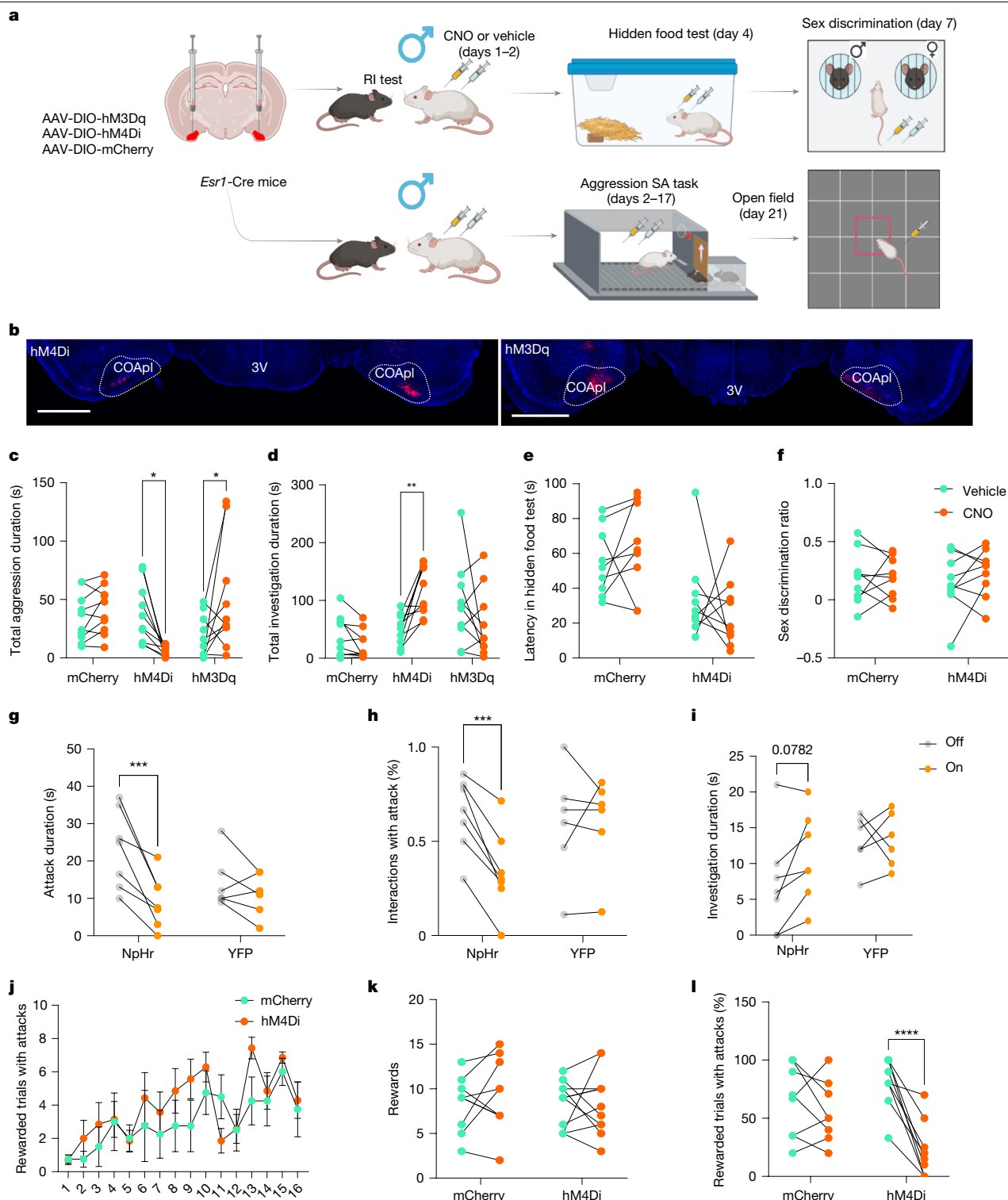


Fig. 3 | Manipulating COAP1^{Esr1} cells alters consummatory drive in male AGCs. **a**, Experimental timeline. **b**, Virus expression in the COAP1. 3V, third ventricle. **c, d**, Inhibition of COAP1^{Esr1} significantly decreased total aggression (**c**; virus × drug interaction: $F_{(2,27)} = 9.687, P = 0.0007$, Sidak's post-hoc $P = 0.0133$) and increased total investigation (**d**; virus × drug interaction: $F_{(2,27)} = 8.305, P = 0.0035$, Sidak's post-hoc $P = 0.0035$). Excitation significantly increased aggression (Sidak's post-hoc $P = 0.0142$) without affecting investigation (Sidak's post-hoc $P = 0.2174$) ($n = 10$ HM4Di, $n = 10$ HM3Dq and $n = 10$ mCherry). **e, f**, Inhibition of COAP1^{Esr1} did not affect the latency to find hidden food (**e**; virus × drug interaction: $F_{(1,16)} = 1.192, P = 0.2911$) or affect sex discrimination (**f**; virus × drug interaction: $F_{(1,16)} = 0.5122, P = 0.4845$) ($n = 9$ HM4Di and $n = 9$ mCherry). **g–i**, Closed-loop optogenetic inhibition reduced total time attacking (**g**; virus × laser interaction: $F_{(1,11)} = 6.838, P = 0.0240$, Sidak's post-hoc $P = 0.0007$),

decreased the percentage of interactions with an attack (**h**; virus × laser interaction: $F_{(1,11)} = 12.84, P = 0.0043$, Sidak's post-hoc $P = 0.0006$) and slightly increased total investigation time (**i**; virus × laser interaction: $F_{(1,11)} = 4.919, P = 0.0485$, Sidak's post-hoc $P = 0.0782$) ($n = 7$ NpHR and $n = 6$ YFP). **j–l**, Social self-administration experiments. Both groups increased the number of rewarded trials with attacks (**j**; main effect of session: $F_{(15,135)} = 5.382, P < 0.0001$). Inhibition had no effect on lever pressing (**k**; virus × drug interaction: $F_{(1,18)} = 0.3147, P = 0.5817$) but led to a significant reduction in the percentage of rewarded trials that led to an attack (**l**; virus × drug interaction: $F_{(1,18)} = 13.60, P = 0.0022$, Sidak's post-hoc $P < 0.0001$) ($n = 11$ HM4Di and $n = 9$ mCherry). * $P < 0.05$, ** $P < 0.01$, *** $P < 0.001$, **** $P < 0.0001$. All data are mean ± s.e.m. Scale bar, 1 mm. Data from **c, d, j–l** were replicated in two cohorts; all other data are from a single cohort. The illustrations in **a** were created with BioRender.

we found that inhibiting COApI^{Esr1} with AAV-DIO-hM4Di increased anogenital investigation and decreased the number of active withdrawals (Extended Data Fig. 7d–f). Because COApI^{Esr1} neurons receive input from the main olfactory bulb^{14,16,17}, we ran two control experiments to ensure that the observed alterations in social behaviour were not due to anosmia. We first ran a hidden food test to assess general olfactory processing¹⁸. In the test, mice are food-restricted overnight and must find a piece of food buried under bedding by using their sense of smell. Inhibiting COApI^{Esr1} neurons did not affect the ability of the mice to locate the food (Fig. 3e). Next, we tested the ability of male AGGs to differentiate between males and females¹⁹. Male AGGs were placed in an open-field arena with a male and a female mouse under wire mesh cups on opposite sides of the arena. We computed a discrimination ratio in which the difference in time spent investigating the male and the female was divided by the total time spent investigating both mice. A negative score indicates more time spent investigating the male, and a positive score indicates more time spent investigating the female. We found that inhibiting COApI^{Esr1} neurons did not affect the males' preference for investigating the female mice (Fig. 3f).

To further support the idea that COApI^{Esr1} neurons have a role in mediating the transition from the appetitive to the consummatory phase of aggression, we performed a closed-loop optogenetic inhibition study. Male mice were injected with AAV-halorhodopsin (NpHR) or AAV-YFP. The laser was turned on as the resident approached the intruder, and was kept on for 10 s. We found that inhibiting COApI^{Esr1} neurons decreased attack behaviour (Fig. 3g,h) and increased investigation (Fig. 3i). We also tested whether optogenetic inhibition of the COApI^{Esr1} neurons altered mating behaviour, but did not find any differences in total mounting duration, number of mounts or investigation while the laser was on (Extended Data Fig. 7m–o). Finally, we tested whether inhibiting COApI^{Esr1} neurons altered the motivation to engage in attack behaviour by using the aggression self-administration paradigm²⁰. We found that both the mCherry and the hM4Di groups learned the task equally well in terms of rewarded trials and the occurrence of attacks (Fig. 3j and Extended Data Fig. 7g). After the acquisition of the task, mice were tested using a counterbalanced injection regimen (clozapine-*N*-oxide (CNO) or saline). We did not observe any difference in lever presses (Fig. 3k) between the two groups on CNO, which suggests that COApI^{Esr1} cells do not affect the reinforcing properties of social interaction. However, we observed a marked decrease in the percentage of rewarded trials that led to an attack (Fig. 3l). We also tested mice on a progressive schedule and did not find a difference in the maximum number of lever presses made for access to an intruder, which suggests that the COApI^{Esr1} cells do not regulate the motivation to work for access to an intruder (Extended Data Fig. 7h). Finally, manipulations of COApI^{Esr1} neurons in female AGGs during the RI test did not affect attack (Extended Data Fig. 8a–c) or investigation behaviours (Extended Data Fig. 8d–f). Collectively, these results suggest that inhibiting COApI^{Esr1} neurons selectively alters the consummatory drive in social interactions in male AGGs.

Inhibiting COApI alters network connectivity

After determining the effect of inhibiting COApI^{Esr1} neurons on aggressive behaviour in males, we sought to investigate how inhibiting this cell population alters the connectivity of the pink module from the AGG network. To this end, we injected eight-week-old male AGGs with AAV-DIO-hM4Di or AAV-DIO-mCherry. After recovery from surgery, all mice were given an injection of CNO before the last RI test and were perfused 90 min later (Fig. 4a). As expected, inhibiting COApI^{Esr1} cells decreased attack duration and increased investigation duration (Fig. 4b,c and Extended Data Fig. 9a–f). Brains were perfused, cleared, imaged and registered to the Allen Brain Atlas. We then constructed a network for each group of mice. For visualization, the clusters were organized according to the original AGG network (pink module) to

ensure that the same brain regions would make up similar clusters in the hM4Di and mCherry networks (Fig. 4d–g). As in the modules from Fig. 1, visual inspection indicated a high degree of interconnectedness between amygdalar and hypothalamic subregions under control mCherry conditions. After inhibition of COApI^{Esr1} cells, we observed high levels of interconnectedness within, but not between, amygdalar and hypothalamic subregions, which is consistent with the data from NONs in Fig. 1. We also found that inhibiting COApI^{Esr1} cells with hM4Di significantly decreased the expression of the pink module, relative to the mCherry group (Fig. 4d). We next determined whether the hM4Di and mCherry networks differed in how well they preserved the pink module in the original AGG network. To this end, we performed a module preservation analysis separately for each network, with the original AGG network serving as the reference network. Using the same metrics as those in Fig. 1, we found that the hM4Di network showed a significant decrease in these metrics compared with the mCherry network (Fig. 4e), which suggests that inhibiting COApI^{Esr1} neurons diminished the preservation of the pink module found in the original network. Of the remaining seven clusters, the hM4Di group only showed a significant decrease in the 'red' cluster (Extended Data Fig. 9g). Notably, this cluster contains regions to which COApI^{Esr1} neurons project, including the bed nucleus of the stria terminalis (BNST), the anteroventral periventricular nucleus and the substantia innominata. When examining FOS counts in individual regions of the pink network, we found that 78% of regions showed a significant reduction in FOS cells after inhibition with hM4Di (Fig. 4h and Extended Data Fig. 9h).

Inhibiting COApI^{Esr1} neuron outputs alters aggression

We next sought to understand the involvement of regions within the pink network downstream of COApI^{Esr1} neurons that contribute to the behavioural effects of local COApI^{Esr1} manipulation (Fig. 5a). We injected HSV-1 (H129 TK-TT) to identify monosynaptic connections in downstream regions within the pink module (Fig. 5b). Many of these regions have previously been shown to promote aggressive behaviour, including the VMH, the medial amygdala (MEA), the CEA and the BNST. Furthermore, we found that COApI^{Esr1} neurons also projected to several regions that are involved in olfaction, such as the piriform cortex (PIR), endopiriform cortex, piriform amygdala area (PAA), post-piriform transition area and anterior olfactory nucleus. Notably, COApI^{Esr1} neurons formed monosynaptic connections with 13 of the 28 regions in the pink module, indicating that many of these regions are both functionally and physically connected (Extended Data Fig. 10a). The monosynaptic nature of these connections was further confirmed by injecting AAV-hSyn-FLEX-mGFP-2A-Synaptophysin-mRuby into COApI^{Esr1} neurons to map the anterograde expression of presynaptic inputs to the VMH and CEA. AAV-DIO-ChR2 was injected into the COApI^{Esr1} neurons and ChR2-assisted ex vivo electrophysiology was performed to confirm that there are functional excitatory inputs in both the VMH and the CEA (Extended Data Fig. 10b–d). In addition, of the 13 connected regions, 12 of them showed a significant decrease in FOS after inhibiting COApI^{Esr1} with DREADDs (Fig. 4h). On the basis of this information, we chose to target the VMH (Fig. 5c), which is necessary for aggressive behaviour, and the CEA (Fig. 5d), which has been shown to modulate jaw movements during biting, a key component of aggressive behaviour. To evaluate whether these circuits alter aggressive behaviour, we injected AAV-DIO-NpHR into COApI^{Esr1} neurons of eight-week-old male AGGs and implanted ferrules into either the VMH or the CEA (Fig. 5e). Four weeks later, mice were tested for two days in the RI test in which the order of testing (laser on or off) was counterbalanced. We found that inhibiting the COApI–CEA pathway resulted in a significant decrease in total attack duration without affecting social investigation (Fig. 5f,g). Alternatively, we found that inhibiting the COApI–VMH pathway produced both a reduction in attack duration and an increase in social investigation, mirroring the effects of local inhibition of COApI^{Esr1} neurons.

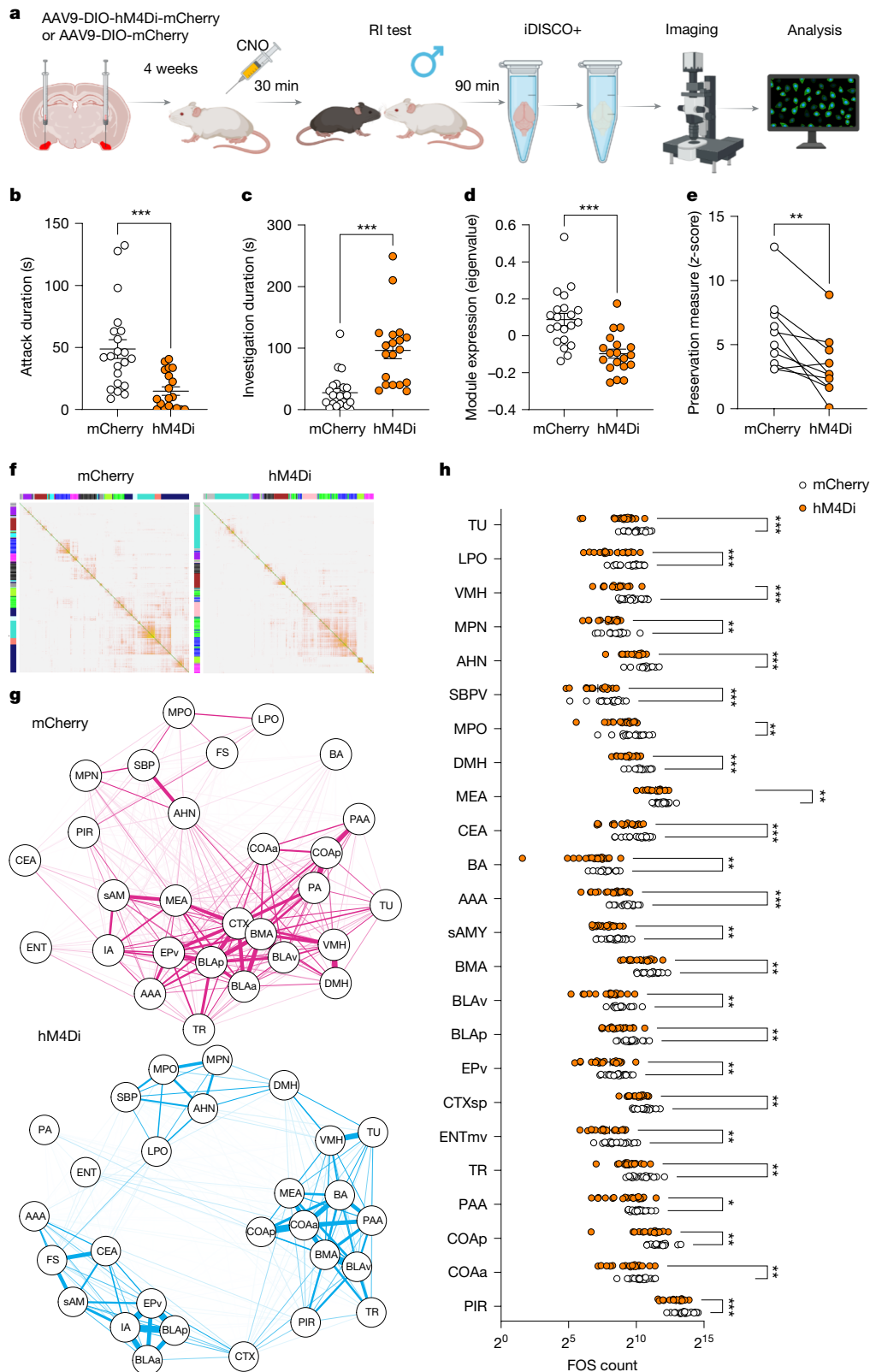


Fig. 4 | Manipulating COAP1^{Esrt} cells alters connectivity in the pink module. **a**, Experimental timeline. **b,c**, Inhibition of COAP1^{Esrt} cells reduces attack duration (**b**; $t_{(38)} = 3.731, P = 0.0006$) and increases investigation duration (**c**; $t_{(38)} = 4.719, P < 0.0001$). **d,e**, The mCherry network showed higher expression of the pink module (**d**; $t_{(38)} = 4.442, P < 0.0001$) when the two networks were combined, and preserved the connectivity and density of the pink module better than the hM4Di network did (**e**; $t_{(9)} = 3.983, P = 0.0032$) when they were separately analysed. Each pair of points connected by a line is a single preservation metric from each network ($n = 19$ (hM4Di) and $n = 21$ (mCherry)). **f**, Whole-brain

FOS network in mice injected with mCherry or hM4Di. **g**, Network plot of the pink module in mice injected with mCherry (top) or with hM4Di (bottom), from the wild-type AGG network. Regions from the mCherry and hM4Di networks were plotted using the colour label from the original network. **h**, Of the 28 regions in the pink module, inhibition of COAP1^{Esrt} cells significantly decreased FOS expression in 24 regions (86%). Network analyses were replicated in two cohorts. * $P < 0.05$, ** $P < 0.01$, *** $P < 0.001$ ($n = 21$ mCherry and $n = 19$ hM4Di). All data are mean \pm s.e.m. The illustrations in **a** were created with BioRender.

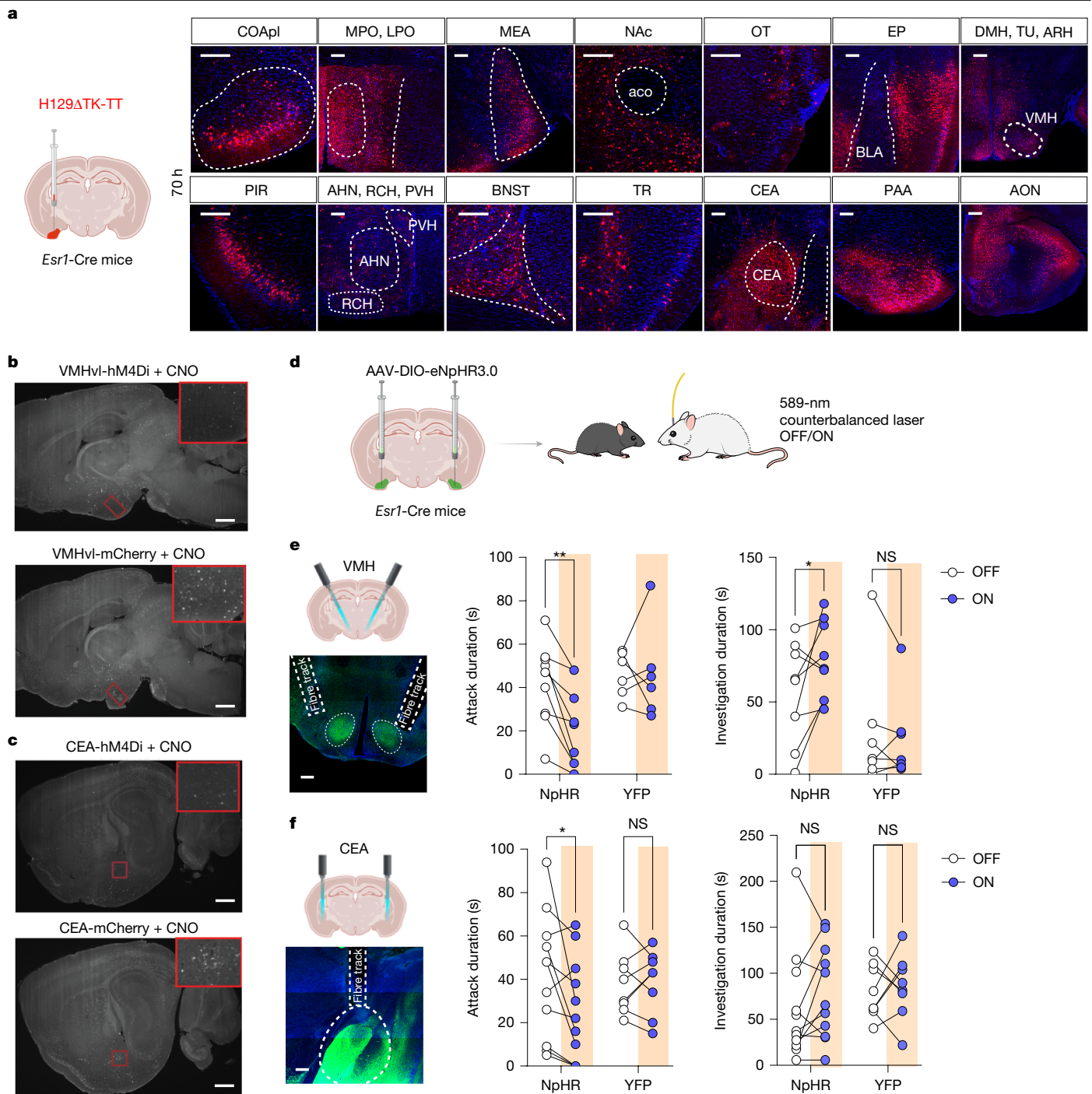


Fig. 5 | Optogenetic inhibition of regions downstream of COApl^{Esr1} cells alters social behaviour in male AGGs. **a**, Schematic of experimental timeline and regions that receive monosynaptic input from COApl^{Esr1} neurons revealed by HSV-1 trans-synaptic anterograde tracing. Scale bar, 100 μ m. **b, c**, Images of FOS⁺ cells in the ventrolateral portion of the VMH (VMHvl) (**b**) and CEA (**c**) from mice injected with hM4Di or mCherry. **d**, Schematic of behavioural set-up. **e**, Inhibition of terminals in the VMH with NpHR reduces attack duration in mice injected (virus \times laser interaction: $F_{(1,14)} = 7.893$, $P = 0.0139$, Sidak's post-hoc $P = 0.0048$) and increases investigation duration (virus \times laser interaction: $F_{(1,14)} = 4.939$, $P = 0.0436$, Sidak's post-hoc $P = 0.0402$). **f**, Inhibition of terminals

in the CEA reduces attack duration in mice injected with NpHR (virus \times laser interaction: $F_{(1,17)} = 3.654$, $P = 0.0729$, Sidak's post-hoc $P = 0.0239$) but has no effect on investigation duration (virus \times laser interaction: $F_{(1,17)} = 0.3555$, $P = 0.5589$, Sidak's post-hoc $P = 0.3696$) ($n = 9$ (VMH NpHR), $n = 7$ (VMH YFP), $n = 11$ (CEA NpHR) and $n = 8$ (CEA YFP)). Scale bar, 200 μ m. * $P < 0.05$, ** $P < 0.01$; NS, not significant. All data are mean \pm s.e.m. The illustrations in **a, d, e, f** were created with BioRender. PVH, paraventricular nucleus of the hypothalamus; NAc, nucleus accumbens; AON, anterior olfactory nucleus; ARH, arcuate nucleus of hypothalamus; OT, olfactory tubercle; EP, endopiriform nucleus.

Discussion

Using an unsupervised approach to analyse whole-brain FOS patterns, we identified COApl as a key region that controls the transition from social investigation to aggressive behaviour in male—but not in

female—mice. Of note, many of the regions that are highly connected to the COApl have previously been identified as part of the 'core aggression circuit'; for example, the MEA, VMH and BNST. Furthermore, many of these regions receive inputs from both the main olfactory bulb (COApl, anterior cortical amygdala (COAa), PIR and PAA) and the

accessory olfactory bulb (MEA and COApm) and project to multiple downstream regions in the hypothalamus¹⁷. Because both of these sensory streams are necessary for aggressive social behaviour^{21,22}, olfactory cues detected by each stream are likely to be detected in parallel and converge in hypothalamic regions such as the VMH to induce specific social behaviours. Given that these regions are clustered together with many other brain regions whose functions have not been examined in the context of aggression, it is possible that the core aggression circuit is larger than previously considered and requires further investigation.

According to our current understanding of the circuitry that mediates aggression, one might predict that a loss-of-function manipulation in the COApl would result in decreased aggression, owing to the lack of social approach^{10,23}. This expectation is perhaps due to previous studies that have shown that loss-of-function manipulations in the main olfactory bulb, which projects to the COApl, reduce social investigation and aggression^{21,22}. However, our findings that COApl^{Esr1} neurons are more active during RI trials in which an attack occurs, and are active specifically during investigation bouts that precede an attack, suggest that this region is not simply relaying olfactory 'cues' to downstream regions. This is further supported by our results showing that inhibiting COApl^{Esr1} neurons increases investigation rather than decreasing it, without resulting in anosmia. In addition, our finding that COApl^{Esr1} neurons respond to odours from conspecifics, but not those from predators, suggests that they are not acting as a simple 'threat detector', which is in line with a previous study that showed that the COApl is not involved in fear responses to predator odour¹⁹. Although it was previously reported that the COApl is required for attraction to non-social odorants such as 2-phenylethanol, these studies were not performed in a cell-type-specific manner¹⁴. Our data support the idea that COApl^{Esr1} neurons are activated exclusively by odours emitted from social conspecifics, and therefore shape the type of social encounter that ensues.

One potential explanation of our findings is that COApl^{Esr1} neurons are involved in the motivation to attack the intruder, thereby regulating the rewarding and reinforcing properties of aggression²⁴ (Extended Data Fig. 11). In support of this explanation, inhibiting COApl^{Esr1} neurons with hm4Di robustly decreased the percentage of rewarded trials that led to an attack in an aggression self-administration task. However, inhibiting COApl^{Esr1} neurons did not change the number of lever presses, and mice in both groups worked equally hard for access to a social target, suggesting that their motivation to interact with the intruder—albeit in a less aggressive and more pro-social way—remained intact. Some previously published studies of other nuclei that make up the pallial amygdala (basolateral, basomedial, cortical and posterior amygdala) support its role in rodent social behaviour^{25–27}. Inhibiting basolateral amygdala (BLA) inputs to the ventral hippocampus and the medial prefrontal cortex increases affiliative social behaviour in mice, although aggression was not assayed in these studies. Conversely, manipulating the posterior amygdala alters aggressive behaviour without affecting pro-social investigation^{28,29}. Pallial amygdala subcircuits have also been implicated in social behaviour in studies of humans and non-human primates. These studies have focused largely on the BLA and the lateral amygdala, given their extensive connections with the visual system^{30,31}, on which primates are highly reliant during social interactions. Some studies have shown that neurons in the BLA fire when primates make eye contact with one another, and bilateral lesions often reduce fear of others and limit aggression. However, some contradictory results have also been reported, perhaps owing to the use of non-specific excitotoxic lesions (reviewed in ref. 32). A study in which the GABA (γ -aminobutyric acid) agonist muscimol was used to reversibly inhibit the BLA increased affiliative behaviours between pairs of rhesus monkeys, whereas activating the BLA resulted in social withdrawals without affecting anxiety³³, mirroring our findings in mice. Furthermore, single-unit recordings in humans indicate that neurons in the amygdala are sensitive to the subjective perception of emotions

shown in facial stimuli, as opposed to just the features of the stimuli³⁴. This suggests that the amygdala of different individuals can respond differently to the same sensory cues depending on the behavioural state or belief of the individual. Collectively, these findings have led to the interpretation that the amygdala has a key role in social perception^{35,36}. Thus, it is tempting to speculate that COApl has a role in the perception of the intruder, which is affected by the 'aggressive state' of the resident. Internal states have previously been shown to bias perception towards specific actions in other areas of rodent research^{12,37–39}. Given the marked sex differences observed, gonadal state might also contribute. Cells that express ESRI are sensitive to oestradiol, and thus, it is possible that sex steroid hormones modify neural circuits that are involved in olfaction, thereby determining how particular odours are interpreted by the animal⁴⁰. For example, gonadectomy eliminates males' preference for receptive female odours and the avoidance of male odours with fighting experience. In the context of aggression, given that AGGs have higher levels of circulating testosterone than do NONs⁴, it is possible that this contributes to the perceived importance of odours from the intruder in a sex-specific way. Together, our research provides a foundation for understanding the neural mechanisms that underlie social perception and action selection. Future studies that aim to delineate the mechanisms by which internal states and perceptual processes interact to execute distinct behaviours during dyadic social interactions will thus be crucial.

Online content

Any methods, additional references, Nature Portfolio reporting summaries, source data, extended data, supplementary information, acknowledgements, peer review information; details of author contributions and competing interests; and statements of data and code availability are available at <https://doi.org/10.1038/s41586-024-08540-4>.

- Craig, W. Appetites and aversions as constituents of instincts. *Biol. Bull.* **34**, 91–107 (1918).
- Hashikawa, K., Hashikawa, Y., Falkner, A. & Lin, D. Y. The neural circuits of mating and fighting in male mice. *Curr. Opin. Neurobiol.* **38**, 27–37 (2016).
- Aubry, A. V. et al. Sex differences in appetitive and reactive aggression. *Neuropsychopharmacology* **47**, 1746–1754 (2022).
- Golden, S. A. et al. Basal forebrain projections to the lateral habenula modulate aggression reward. *Nature* **534**, 688–692 (2016).
- Flanigan, M. E. et al. Orexin signaling in GABAergic lateral habenula neurons modulates aggressive behavior in male mice. *Nat. Neurosci.* **23**, 638–650 (2020).
- Aleyasin, H. et al. Cell-type-specific role of Δ FosB in nucleus accumbens in modulating intermale aggression. *J. Neurosci.* **38**, 5913–5924 (2018).
- Takahashi, A. et al. Neuromodulatory effect of interleukin 1 β in the dorsal raphe nucleus on individual differences in aggression. *Mol. Psychiatry* **27**, 2563–2579 (2022).
- Lin, D. et al. Functional identification of an aggression locus in the mouse hypothalamus. *Nature* **470**, 221–226 (2011).
- Lee, H. et al. Scalable control of mounting and attack by Esr1⁺ neurons in the ventromedial hypothalamus. *Nature* **509**, 627–632 (2014).
- Lischinsky, J. E. & Lin, D. Neural mechanisms of aggression across species. *Nat. Neurosci.* **23**, 1317–1328 (2020).
- Oettl, L. L. et al. Oxytocin enhances social recognition by modulating cortical control of early olfactory processing. *Neuron* **90**, 609–621 (2016).
- Marlin, B. J. et al. Oxytocin enables maternal behaviour by balancing cortical inhibition. *Nature* **520**, 499–504 (2015).
- Renier, N. et al. iDISCO: a simple, rapid method to immunolabel large tissue samples for volume imaging. *Cell* **159**, 896–910 (2014).
- Root, C. M., Denny, C. A., Hen, R. & Axel, R. The participation of cortical amygdala in innate, odour-driven behaviour. *Nature* **515**, 269–273 (2014).
- McGregor, A. & Herbert, J. Differential effects of excitotoxic basolateral and corticomedial lesions of the amygdala on the behavioural and endocrine responses to either sexual or aggression-promoting stimuli in the male rat. *Brain Res.* **574**, 9–20 (1992).
- Miyamichi, K. et al. Cortical representations of olfactory input by trans-synaptic tracing. *Nature* **472**, 191–196 (2011).
- Sosulski, D. L., Bloom, M. L., Cutforth, T., Axel, R. & Datta, S. R. Distinct representations of olfactory information in different cortical centres. *Nature* **472**, 213–216 (2011).
- Yang, M. & Crawley, J. N. Simple behavioral assessment of mouse olfaction. *Curr. Protoc. Neurosci.* **48**, 8.24.1–8.24.12 (2009).
- Pankevich, D. E., Baum, M. J. & Cherry, J. A. Olfactory sex discrimination persists, whereas the preference for urinary odorants from estrous females disappears in male mice after vomeronasal organ removal. *J. Neurosci.* **24**, 9451–9457 (2004).
- Golden, S. A. et al. Nucleus accumbens Drd1-expressing neurons control aggression self-administration and aggression seeking in mice. *J. Neurosci.* **39**, 2482–2496 (2019).

21. Stowers, L., Holy, T. E., Meister, M., Dulac, C. & Koentges, G. Loss of sex discrimination and male–male aggression in mice deficient for TRP2. *Science* **295**, 1493–1500 (2002).
22. Mandiyan, V. S., Coats, J. K. & Shah, N. M. Deficits in sexual and aggressive behaviors in *Cnga2* mutant mice. *Nat. Neurosci.* **8**, 1660–1662 (2005).
23. Wei, D., Talwar, V. & Lin, D. Neural circuits of social behaviors: innate yet flexible. *Neuron* **109**, 1600–1620 (2021).
24. Aleyasin, H., Flanigan, M. E. & Russo, S. J. Neurocircuitry of aggression and aggression seeking behavior: nose poking into brain circuitry controlling aggression. *Curr. Opin. Neurobiol.* **49**, 184–191 (2018).
25. Felix-Ortiz, A. C. & Tye, K. M. Amygdala inputs to the ventral hippocampus bidirectionally modulate social behavior. *J. Neurosci.* **34**, 586–595 (2014).
26. Huang, W. C., Zucca, A., Levy, J. & Page, D. T. Social behavior is modulated by valence-encoding mPFC–amygdala sub-circuitry. *Cell Rep.* **32**, 107899 (2020).
27. Kwon, J. T. et al. An amygdala circuit that suppresses social engagement. *Nature* **593**, 114–118 (2021).
28. Yamaguchi, T. et al. Posterior amygdala regulates sexual and aggressive behaviors in male mice. *Nat. Neurosci.* **23**, 1111–1124 (2020).
29. Zha, X. et al. VMHvl-projecting *Vglut1*⁺ neurons in the posterior amygdala gate territorial aggression. *Cell Rep.* **31**, 107517 (2020).
30. Vuilleumier, P., Richardson, M. P., Armony, J. L., Driver, J. & Dolan, R. J. Distant influences of amygdala lesion on visual cortical activation during emotional face processing. *Nat. Neurosci.* **7**, 1271–1278 (2004).
31. Amaral, D. G., Behniea, H. & Kelly, J. L. Topographic organization of projections from the amygdala to the visual cortex in the macaque monkey. *Neuroscience* **118**, 1099–1120 (2003).
32. Gothard, K. M. Multidimensional processing in the amygdala. *Nat. Rev. Neurosci.* **21**, 565–575 (2020).
33. Wellman, L. L., Forcelli, P. A., Aguilar, B. L. & Malkova, L. Bidirectional control of social behavior by activity within basolateral and central amygdala of primates. *J. Neurosci.* **36**, 8746–8756 (2016).
34. Wang, S. et al. Neurons in the human amygdala selective for perceived emotion. *Proc. Natl Acad. Sci. USA* **111**, E3110–E3119 (2014).
35. Rutishauser, U., Mamelak, A. N. & Adolphs, R. The primate amygdala in social perception - insights from electrophysiological recordings and stimulation. *Trends Neurosci.* **38**, 295–306 (2015).
36. Gangopadhyay, P., Chawla, M., Dal Monte, O. & Chang, S. W. C. Prefrontal–amygdala circuits in social decision-making. *Nat. Neurosci.* **24**, 5–18 (2021).
37. Livneh, Y. et al. Homeostatic circuits selectively gate food cue responses in insular cortex. *Nature* **546**, 611–616 (2017).
38. Burgess, C. R. et al. Hunger-dependent enhancement of food cue responses in mouse postnatal cortex and lateral amygdala. *Neuron* **91**, 1154–1169 (2016).
39. Schiavo, J. K. et al. Innate and plastic mechanisms for maternal behaviour in auditory cortex. *Nature* **587**, 426–431 (2020).
40. Gandelman, R. Gonadal hormones and sensory function. *Neurosci. Biobehav. Rev.* **7**, 1–17 (1983).

Publisher's note Springer Nature remains neutral with regard to jurisdictional claims in published maps and institutional affiliations.



Open Access This article is licensed under a Creative Commons Attribution-NonCommercial-NoDerivatives 4.0 International License, which permits any non-commercial use, sharing, distribution and reproduction in any medium or format, as long as you give appropriate credit to the original author(s) and the source, provide a link to the Creative Commons licence, and indicate if you modified the licensed material. You do not have permission under this licence to share adapted material derived from this article or parts of it. The images or other third party material in this article are included in the article's Creative Commons licence, unless indicated otherwise in a credit line to the material. If material is not included in the article's Creative Commons licence and your intended use is not permitted by statutory regulation or exceeds the permitted use, you will need to obtain permission directly from the copyright holder. To view a copy of this licence, visit <http://creativecommons.org/licenses/by-nc-nd/4.0/>.

© The Author(s) 2025

Article

Methods

Mice

Wild-type Swiss-Webster (SW) mice (male and female, 12–15 weeks; Charles River) and *Esr1*-Cre mice (017911, B6N.129S6(Cg)-*Esr1*^{tm1.1(cre)And}/J; Jackson Laboratory) were crossed with SW females to obtain F₁ mice used as experimental mice. Intruders for the RI test were 8–12-week-old male or female C57/BL6J mice (Jackson Laboratory). All delivered mice were allowed one week of acclimation to the housing facility before any experimental protocol. At four weeks, mice were separated from their littermates and paired with a member of the opposite sex for sexual experience for two days at eight weeks of age. Females were paired with castrated SW males (8–12 weeks; Charles River) to prevent pregnancy. All mice were maintained on a 12 h–12 h light–dark cycle (07:00–19:00) with ad libitum access to food and water. Housing and experimental rooms were maintained at 20–22 °C and 40–60% humidity. Experiments were performed during the light phase. Animals were randomly assigned to groups, arena or treatments, and data analysis was done in a double-blind fashion. Sample sizes were chosen according to experience and historical studies. Procedures were performed in accordance with the National Institutes of Health Guide for Care and Use of Laboratory Animals and were approved by the Icahn School of Medicine at Mount Sinai Institutional Animal Care and Use Committee.

RI test

Mice were screened using protocols adapted from previous studies^{3,41,42}. In brief, cage tops were removed and replaced with plexiglass covers to monitor trials. A novel C57BL/6J mouse matching the sex of the resident was introduced into each cage and mice were allowed to freely interact for 5 min. After this, intruder mice were returned to their home cages and, in the case of female RI trials, cohabiting male mice were returned to their home cages. For the male mating assay, SW female intruders were pre-screened for sexual receptivity. All assays lasted 10 min and intruder mice were returned to their home cages at the end of the session. All videos were recorded for later analysis. Resident behaviours were manually annotated using Observer XT 11.5 (Noldus Interactive Technologies).

Aggression self-administration test

Aggression self-administration testing was performed as previously described. In brief, SW resident mice were placed in standard Med Associates operant chambers and underwent eight trials per day for 16 days in which they could press a lever (FR1) to receive access to a subordinate same-sex mouse through a guillotine door into their operant chamber. A house light illuminated the chambers during trials, and an inactive lever was extended at all times. At the beginning of a trial, the house light was turned on, and a lever was extended 10 s later. If the resident pressed for a reward, a 2-s tone played and a guillotine door next to the active lever opened for 12 s. A same-sex C57BL/6J intruder manually pushed into the chamber, and the intruder was removed at the end of the trial. If residents did not press, the active lever retracted after 60 s. All chambers also had recessed food pellet receptacles with beam-break registered entry ports. We performed all progressive ratio (PR) tests using the same parameters as those in self-administration training, except for the trial design. After reward obtaining (number of required active lever presses for a given trial), the automatic guillotine door was opened for 10 s and the same-sex intruder (C57BL/6J) was manually pushed inside the main operant chamber. Immediately after the automatic door closed, the active–inactive levers were re-extended. The intruder mouse was removed from the chamber after an attack or after 30 s had elapsed. The PR session was terminated if no reinforced responses occurred after a total duration of 20 min had elapsed. Throughout the sessions, for each trial, the number of responses required to activate the guillotine door and gain access to

the intruder was incremented following an exponential progression ($R = (5 \times e^{0.12P}) - 5$, where P is the previous ratio). The breakpoint value corresponds to the total number of rewards (number access to the intruder during the whole session). *Esr1*-cre mice transfected in the COAP1 with AAV9-DIO-hm4Di-mCherry or AAV9-DIO-mCherry (see below for titre, surgery information and coordinates) were administered either saline or CNO, counterbalanced over the two days of the PR. Acquisition of self-administration was monitored in one of two cohorts. The data in Fig. 3j are from cohort 2.

Hidden food test

Mice were habituated to and allowed to consume a palatable food (a Reese's mini peanut butter cup) two days before being tested. Mice were then food-restricted the night before the test. Mice were tested under red light and placed in a clean cage. The food was placed 8 cm deep in the bedding of the cage and the time to find the food was recorded with a stopwatch.

Sex discrimination test

Male and female C57BL/6J mice were used as target mice and placed on opposite sides of an open-field enclosure in mesh cups. Test mice were placed in the open field and allowed to explore the arena for five minutes under red light. Mice were recorded with an overhead Ethovision camera and the time spent interacting with each mouse was scored offline manually. To calculate the discrimination ratio, the total time spent interacting with both mice was divided by the difference between the time spent with the female and male. A positive discrimination ratio indicates more time spent with the female, and a negative ratio indicates more time spent with the male.

Perfusion and brain-tissue processing

For iDISCO+, mice were injected with 10% chloral hydrate and perfused transcardially with ice-cold 1× phosphate-buffered saline (PBS) (pH 7.4), followed by fixation with cold 4% paraformaldehyde in 1× PBS. Brains were post-fixed for 12 h in the same fixative at 4 °C. For FISH, brains were rapidly removed and flash-frozen in –30 °C isopentane for 5–10 s, then kept at –80 °C until sectioning. Slices were sectioned at 15 μm using a cryostat (Leica). Mice injected with H129ΔTK-TT were perfused 48 or 70 h after injection.

Histology and imaging

For FISH, RNAscope Multiplex Fluorescent Kits (Advanced Cell Diagnostics) were used according to the manufacturer's instructions. Fresh-frozen brains were mounted on slides at a thickness of 15 μm, fixed for 15 min in cold 4% PFA and dehydrated serially with 50%, 70% and 100% EtOH/H₂O for 2 min each, followed by 20 min Protease IV (RNAscope) treatment. Proprietary probes (Advanced Cell Diagnostics) for *Fos* (316921, accession no. NM_010234.2), *Vglut1* (also known as *Slc17a7*) (SLC17A7-C3, accession no. NM_182993.2) and *Esr1* (478201-C2, accession no. NM_007956.5) were hybridized at 40 °C for 2 h, then subjected to a series of amplification steps at 40 °C (1-FL, 30 min; 2-FL, 15 min; 3-FL, 30 min; 4-FL, 15 min). Reagent Alt-A was used for the fourth amplification step, with channel 1 at 488 nm, channel 2 at 550 nm and channel 3 at 647 nm. Finally, slides were treated for 30 s with DAPI and immediately coverslipped with Eco-Mount. All slices were imaged using a Zeiss LSM 780 confocal microscope. Cells from all ISH images (two per sample) were counted blindly across groups at 20×. Cells with at least five puncta for each probe were considered to be positive for the probe of interest. Cell nuclei were counted by creating a 16-bit grey-scale image of the DAPI channel. A threshold was created and nuclei were counted using the 'analyze particles' plug-in. Two sections per sample were analysed for quantification of mRuby⁺ puncta at 40× using the 'analyze particles' function. Each section contained three or four optical sections at 4-μm intervals. Starter cells from two sections were manually counted.

iDISCO+ staining, imaging and ClearMap analysis

The iDISCO+ staining protocol was modified from <http://www.idisco.info> (ref. 43). Fixed whole brains were incubated with the primary FOS antibody (226003, 1:1,000, Synaptic Systems) and secondary donkey anti-rabbit IgG (H+L) highly cross-adsorbed secondary antibody, Alexa Fluor 647 (A-31573, 1:1,000, Thermo Fisher Scientific) for seven days each. A LaVision light-sheet microscope with zoom body was used for half-brain sagittal scanning, with dynamic focus and a step size of 4 μm . Cleared brains were processed as previously described using ClearMap¹³. FOS⁺ cells were quantified using the cell detection module, with cell detection parameters optimized and validated according to the intensity and shape parameters of the signal. The autofluorescence channel was aligned to the Allen Institute's Common Coordinate Framework using the Elastix toolbox. To compare cell counts between AGGs and NONs in both sexes and hM4Di versus mCherry, a negative binomial regression was applied using the `glm.nb` function from the MASS package in R. Group classifications were dummy coded (0 for the AGG group and 1 for the NON group). The maximum-likelihood coefficients α and β were determined through iterative reweighted least squares. A significant β means that group status is related to cell count number at the specified region of interest. z -scores correspond to this β coefficient, normalized by its sample standard deviation. P values were corrected for multiple comparisons using the Benjamini–Hochberg procedure to decrease the false discovery rate. q values below 0.05 were considered significant. For network analysis, the data were expanded to 480 brain regions. For glm analysis, the data were collapsed to 271 regions.

Stereotaxic surgery and viral-gene transfer

Esr1-Cre mice (8–10 weeks old) were anaesthetized with an intraperitoneal injection of ketamine HCl (100 mg kg^{-1}) and xylazine (10 mg kg^{-1}) and positioned on a stereotaxic instrument (David Kopf Instruments). In the lateral portion of the COAp (COApl) (bregma: AP -1.7 mm; ML ± 2.8 mm; DV -5.9 mm), 0.3 μl of virus was bilaterally infused using 33-gauge Hamilton needles over 5 min, with needles left in place for 5 min after injection. For virus delivery, 0.3 μl of AAV8-hSyn-DIO-hM3D-mCherry (2.0×10^{12} vg ml^{-1} , no. 44361-AAV8, Addgene), AAV9-hSyn-DIO-hM4D-mCherry (2.0×10^{12} vg ml^{-1} , no. 44362-AAV9, Addgene) or AAV9-hSyn-DIO-mCherry (2.0×10^{12} vg ml^{-1} , no. 50459-AAV9, Addgene) was injected into the COApl. We also injected 0.3 μl AAV9-hSyn-DIO-hM4D-mCherry (2.0×10^{12} vg ml^{-1} , no. 44362-AAV9, Addgene) into the COApm (bregma: AP -2.4 mm; ML ± 2.0 mm; DV -5.6 mm). For anterograde tracing, 0.3 μl of AAV1-hSyn-FLEX-mGFP-2A-Synaptophysin-mRuby (3×10^{12} vg ml^{-1} , no. 7161-AAV1, Addgene) or 0.2 μl of H129 Δ TK-TT (4.0×10^9 vg ml^{-1} , Center for Neuroanatomy with Neurotropic Viruses) was injected unilaterally into the COApl. For optogenetic manipulations, AAV9-Ef1a-DIO-eNpHR3.0-YFP (3.0×10^{12} vg ml^{-1} , no. 26966-AAV9, Addgene) or AAV9-EF1a-DIO-YFP (3.0×10^{12} vg ml^{-1} , no. 20298-AAV9, Addgene) was injected into the COApl. All AAV injections were performed three to four weeks before behavioural experiments. For optogenetic (NpHR) and FP experiments, cannulae (NpHR: MFC_200/240-0.22_3mm_MF1.25_FLT; FP: MFC_200/250-0.57_3mm_MF1.25_FLT) were implanted at the same time as viral delivery (for COApl local, fibres were implanted 0.2 mm above the injection site). For optogenetic (eNpHR3.0) experiments of COApl terminal stimulation, cannulae (MFC_200/240-0.22_MF1.25_FLT, 6 mm for VMHvl, 5 mm for CEA) were bilaterally implanted into the VMHvl (from bregma: AP -1.7 mm; ML ± 2.5 mm; DV -5.5 mm, 20° angle), or CEA (from bregma: AP -1.5 mm; ML ± 2.5 mm; DV -4 mm, 0° angle). For secure fixture of the optic fibre, dental cement (Grip cement; Dentsply) was added to the skull and around the fibres.

DREADD manipulation

CNO (1 mg kg^{-1} , Tocris) was given intraperitoneally 30 min before the RI test, open field, aggression self-administration, hidden food and sex discrimination tests.

Optogenetics manipulation

For yellow (eNpHR3.0) light stimulation, optical fibres (BFP(2)_200/220/900-0.22_4m_FCM-2xMF1.25, Doric Lenses) were connected to a 589-nm yellow laser diode (no. MGL-III-589-50mW, Opto Engine LLC) using a patch cord with a FC/PC adaptor (no. MFP_200/240/900-0.22_4m_FC-MF1.25, Doric Lenses). A function generator (no. 33220A, Agilent Technologies) was used to generate constant yellow light for eNpHR3.0 experiments during the five-minute RI test. For all optogenetics tests, experimental mice were habituated to patch cords for two days before testing in RI. For RI experiments, mice were tested over two days, counterbalanced under laser-on and laser-off conditions. For closed-loop behavioural experiments, the laser was turned on for 10 s as the resident initiated approach of the intruder for every other approach bout in a counterbalanced manner. Attack behaviour was quantified during the period when the light was on. For mating experiments, the light was left on for the duration of the experiment.

Fibre photometry

Fibre photometry was performed according to the Neurophotometrics manual and published protocols⁵. A fibre-optic patch cord was attached to the implanted cannula with cubic zirconia sleeves covered with black tubing. The opposite end of the cable was coupled to a Neurophotometrics LED port. The open-source Bonsai programme was used to control the system; 470-nm and 415-nm LED lights were used for GCaMP6s signal and autofluorescence measurement. Light at the fibre tip ranged from 40 μW to 80 μW and was constant across trials over testing days. Simultaneous recording of 40 fps from both the 470-nm and the 415-nm channel was achieved phase-to-phase and visualized using Bonsai. Three weeks after virus injection and ferrule implantation, mice were tested in the RI test and were presented with different odours in a counterbalanced manner. Once connected to the apparatus, mice were allowed to rest and habituate for 3–5 min before starting. For the RI test and odour presentation, we recorded Ca²⁺ fluorescence during 2 min of baseline activity without an intruder, followed by 5 min of intruder or odour exposure. The 415-nm channel served as the control channel and was subtracted from the GCaMP6s channel to eliminate autofluorescence, bleaching and motion effects. Change in fluorescence ($\Delta F/F$) was computed by subtracting the average value during the final minute of baseline recording and then dividing the resulting value by the averaged value during the final minute of baseline. This value was then z -scored by subtracting the average $\Delta F/F$ from each value and dividing by the standard deviation. Behavioural data were manually annotated in Ethovision and time stamps were aligned with fluorescence recording.

LFP recordings

Esr1-Cre \times SW male mice (around three to four months old) were anaesthetized using a mix of ketamine and xylazine, and placed in a stereotaxic apparatus (David Kopf). After exposing the skull, custom-made platinum–iridium depth electrodes (Pinnacle Technology) were implanted in the CoApl (from bregma: AP -1.7 mm; ML ± 2.8 mm; DV -5.7 mm) in the VMH (from bregma: AP -1.7 mm; ML ± 0.7 mm; DV -5.8 mm). Before implantation, the electrodes were coated with Vybrant Dil cell-labelling solution (Invitrogen) to later check for the placement of the electrode. Two skull screws (0.25 cm, Pinnacle Technology) were implanted over the left and right cerebellum to serve as ground and common reference for recording LFPs. Electrodes and reference screws were connected to a 6-pin connector for mice (Pinnacle Technology) and sealed using dental cement (Metabond). After surgery, mice recovered for at least one week in standard housing conditions before behavioural testing. All recordings were performed in the mouse home cage and the behavioural sessions were videotaped with an overhead camera connected to Ethovision 15 (Noldus). A transistor–transistor logic signal was sent through Ethovision to the LFP acquisition software

Article

to synchronize behavioural and neurophysiological data. LFP signals were captured using a tethered data acquisition system (Model 8401HS, Pinnacle Technology) and acquired using Sirenia Acquisition software (Pinnacle Technology). Data were acquired at 2 kHz using a Pinnacle Technology preamplifier (gain $\times 100$) and with high-pass (0.5 Hz) and low-pass (200 Hz) filters. Signals were segmented into single trial epochs aligned to stimulus-onset.

LFP analysis

Raw data files were loaded into R and analysed with the PSD package⁴⁴. The signal was low-pass-filtered up to 200 Hz using a Butterworth filter before analyses. Signal from the first two seconds of an attack or investigation bout that did not precede an attack was selected for analysis. We chose the first two seconds because all behaviours of interest lasted at least two seconds. A fast Fourier transform with multiple sine tapers⁴⁵ was performed on each segment. Data were then bandpass-filtered for the delta (1–4 Hz), theta (5–12 Hz) and gamma (40–100 Hz) frequency bands. Coherency (defined as the cross-spectral density divided by the auto-spectral density) values were computed from 0 Hz to 100 Hz using the `pspectrum` function for each event and averaged across all events for each value. Coherency values from a one-minute baseline period were subtracted from the coherency values obtained during social behaviours.

Ex vivo electrophysiology

For recording optically evoked excitatory postsynaptic currents (oEPSCs), AAV9-EF1a-DIO-ChR2-eYFP (0.5 μ l, 3.0×10^{12} vg ml⁻¹, Addgene, 35509-AAV9) was injected unilaterally into the COApl of eight-week-old male *Esr1-Cre* mice. At five to eight weeks after injection, coronal brain slices of the VMH and CEA were prepared using a Compressstome (no. VF-210-OZ, Precisionary Instruments) in cold (0–4 °C) sucrose-based artificial cerebrospinal fluid (aCSF) containing 87 mM NaCl, 2.5 mM KCl, 1.25 mM NaH₂PO₄, 4 mM MgCl₂, 23 mM NaHCO₃, 75 mM sucrose and 25 mM glucose. Slices were transferred to a recording chamber continuously perfused at 2–3 ml min⁻¹ with oxygenated aCSF. Patch pipettes (4–7 M Ω) were pulled from thin-walled borosilicate glass using a micropipette puller (P-97, Sutter Instruments) and filled with a potassium gluconate (KGlu)-based intrapipette solution containing 116 mM KGlu, 20 mM HEPES, 0.5 mM EGTA, 6 mM KCl, 2 mM NaCl, 4 mM ATP, 0.3 mM GTP and 2 mg ml⁻¹ biocytin (pH adjusted to 7.2). Cells were visualized using an upright microscope with an IR-DIC lens and illuminated with a white light source (Scientifica). Illumination with a 470-nm LED (pE-300ultra, CoolLED) through the microscope objective was used for visualizing eYFP⁺ cells. VMH and CEA neurons were recorded in voltage-clamp mode. COApl^{ESr1} terminals were stimulated through the microscope $\times 40$ objective (5 ms per pulse, 470 nm; pE-300ultra, CoolLED). oEPSCs were recorded at -70 mV in the presence of tetrodotoxin (TTX, 1 μ M, Tocris) and 4-aminopyridine (100 μ M, Tocris) to probe monosynaptic effects. oEPSCs were blocked by bath application of NBQX (no. SR-95531, 5 μ M, Tocris) confirming the glutamatergic nature of the synaptic contact. Whole-cell recordings were performed using a patch-clamp amplifier (Axoclamp 200B, Molecular Devices) connected to a Digidata 1550 LowNoise acquisition system (Molecular Devices). Signals were low-pass-filtered (Bessel, 2 kHz) and collected at 10 kHz using the data acquisition software pCLAMP 11 (Molecular Devices). Electrophysiological recordings were extracted and analysed using Clampfit (Molecular Devices).

Weighted correlation network analysis

For network construction, we followed previously published guidelines⁴⁶. In brief, an $n \times n$ adjacency matrix was created that encodes the connection strengths between pairs of nodes (brain regions), using the power adjacency function: $A_{ij} = |s_{ij}|^\beta$. A_{ij} refers to the adjacency matrix and s_{ij} refers to the correlation between regions i and j raised to the

power of β . The correlation is raised to the power of β to reduce the influence of potentially spurious correlations. To measure the similarity between the nodes for clustering, the topological overlap measure (TOM) was used: $\omega_{i,j} = \frac{l_{ij} + a_{ij}}{\min\{k_i, k_j\} + 1 - a_{ij}}$. $\omega_{i,j}$ refers to the TOM matrix, $l_{ij} = \sum_u a_{iu}a_{uj}$ and $a_{ij} = |s_{ij}|^\beta$. In words, this is the sum of the product of the shared connections between regions i and j plus the direct connection between regions i and j . This value is divided by the denominator to achieve a value between 0 and 1. To compare the expression of these modules between sexes within a network, a singular value decomposition (SVD) was computed on each module. The SVD is defined as: $X^n = U \times S \times V^T$. X^n is the TOM matrix for the n th module in the network, U and V^T are matrices of orthonormal vectors and S is a diagonal matrix of eigenvalues that denote how much variation is accounted for by each column of U and V . To determine which modules differed between the AGG and NON networks, or whether the mCherry and hM4Di networks conserved module connectivity and density, we used the module preservation function. For comparisons between networks we focused on the following measures for connectivity: Z.cor.KIM, Z.cor.KME, Z.cor.KMEall, Z.cor.cor and Z.cor.MAR. For density measures, we focused on Z.propVarExplained, Z.meanSignAwareCorDat, Z.meanAdj and Z.mean.MAR. All z values were derived by randomly permuting the module labels in the test network and calculating the corresponding preservation metric. The average value of each statistic from the permutations is subtracted from the observed statistic and divided by the standard deviation of the statistic from the permutations. For a detailed explanation of the preservation measures, see Supplementary Table 2. All of the above steps were performed using the WGCNA package in R.

Statistical analysis

All statistical tests and associated information are reported in the figure legends. All t -tests, one- and two-way ANOVAs were performed using GraphPad Prism software. Two-way ANOVA analysis was followed by Šidák's or Tukey's multiple-comparisons test for post-hoc analysis. One-way mixed-effects ANOVA was followed by Tukey's post-hoc test. For comparisons between groups for region by region iDISCO+ analysis, P values were corrected for multiple comparisons using the Benjamini–Hochberg procedure to reduce the false discovery rate. q values below 0.05 were considered significant.

Reporting summary

Further information on research design is available in the Nature Portfolio Reporting Summary linked to this article.

Data availability

All data for animal behaviours, ISH, fibre photometry and LFPs are available with this paper. Source data are provided with this paper.

- Li, L. et al. Social trauma engages lateral septum circuitry to occlude social reward. *Nature* **613**, 696–703 (2023).
- Golden, S. A. et al. Compulsive addiction-like aggressive behavior in mice. *Biol. Psychiatry* **82**, 239–248 (2017).
- Renier, N. et al. Mapping of brain activity by automated volume analysis of immediate early genes. *Cell* **165**, 1789–1802 (2016).
- Barbour, A. J. & Parker, R. L. psd: Adaptive, sine multitaper power spectral density estimation for R. *Comput. Geosci.* **63**, 1–8 (2014).
- Riedel, K. S. & Sidorenko, A. Minimum bias multiple taper spectral estimation. *IEEE Trans. Signal Process.* **43**, 188–195 (1995).
- Langfelder, P. & Horvath, S. WGCNA: an R package for weighted correlation network analysis. *BMC Bioinformatics* **9**, 559 (2008).

Acknowledgements We thank A. Smith for help with the iDISCO+ protocol and ClearMap analysis, and N. Tzavaras, K. Cialowicz and G. Doherty for help with light-sheet imaging. This work was supported by the US National Institutes of Health (grants R01MH114882, R01MH127820, R01MH104559, R01MH120514 and R01MH120637 to S.J.R., K99DK137037 to K.L.C. and K99DA058213 to A.V.A.); the DofT family in the Friedman Brain Institutes' Postdoc Innovator award (A.V.A.); the Brain and Behavior Research Foundation (grants 30233 to L.L., 31140 to

R.D.-d.C., 30894 to K.L.C., 31194 to L.F.P. and 29104 to F.C.); the Beijing Natural Science Foundation (grant Z240012 to L.L.); the Canadian Institutes of Health Research (grant 201811MFE-414896-231226 to K.L.C., R01MH118297 to H.M.); and the NIH Virus Center (grant P40 OD010996).

Author contributions A.V.A., L.L. and S.J.R. conceived the project and designed all experiments. Surgeries were performed by L.L., R.D.-d.C., L.F.P. and C.J.B. Tissue preparation was performed by L.L., R.D.-d.C., E.K., C.J.B., F.C., L.F.P., K.L.C., Y.Y., C.Y., F.D., A.T., J.A. and H.-y.L. FISH, microscopy imaging and analysis, fibre photometry, DREADD and optogenetics data collection were performed by L.L., A.V.A. and R.D.-d.C., and all of the following analysis was performed by A.V.A. LFP experiments were performed by R.D.-d.C., A.V.A. and T.N. Social self-administration experiments were performed by A.V.A., R.D.-d.C., R.L.F.-F., K.T.W., A.R.L. and L.L. iDISCO+ procedures were performed by L.L., R.D.-d.C. and E.K. A.V.A. analysed data generated by ClearMap. A.V.A. constructed weighted correlation network analysis networks and performed

preservation analysis. R.C.F. and H.M. provided intellectual input and edited the manuscript. The results were interpreted by A.V.A., R.D.-d.C., L.L. and S.J.R. The manuscript was written by A.V.A. and S.J.R. and edited by all authors.

Competing interests The authors declare no competing interests.

Additional information

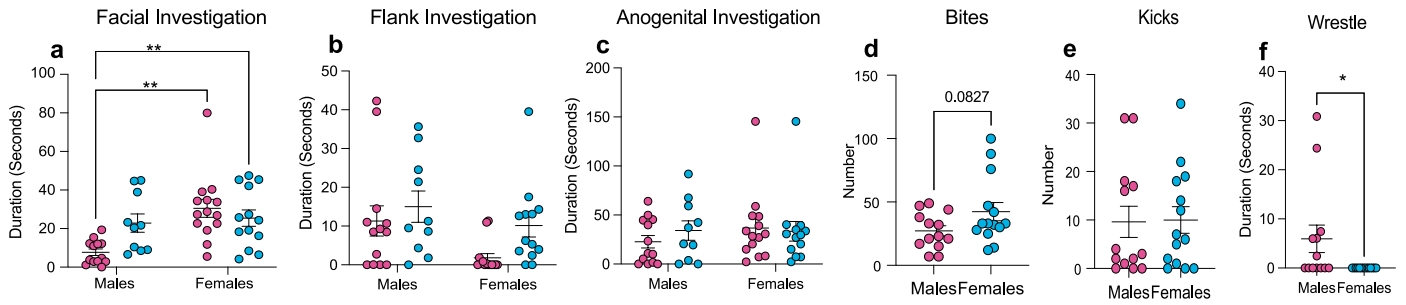
Supplementary information The online version contains supplementary material available at <https://doi.org/10.1038/s41586-024-08540-4>.

Correspondence and requests for materials should be addressed to Long Li or Scott J. Russo.

Peer review information *Nature* thanks Alfred Robison and the other, anonymous, reviewer(s) for their contribution to the peer review of this work. Peer reviewer reports are available.

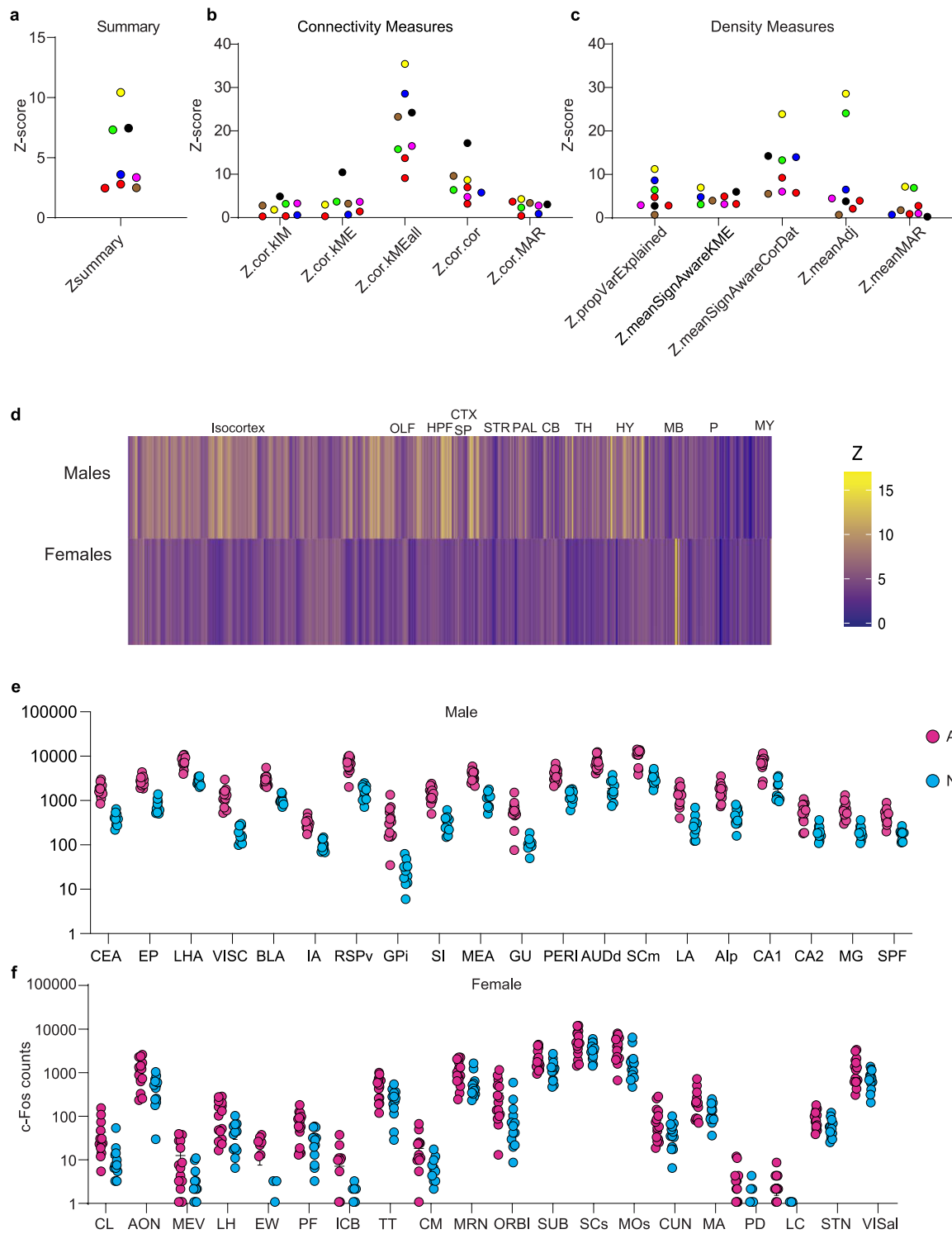
Reprints and permissions information is available at <http://www.nature.com/reprints>.

Article



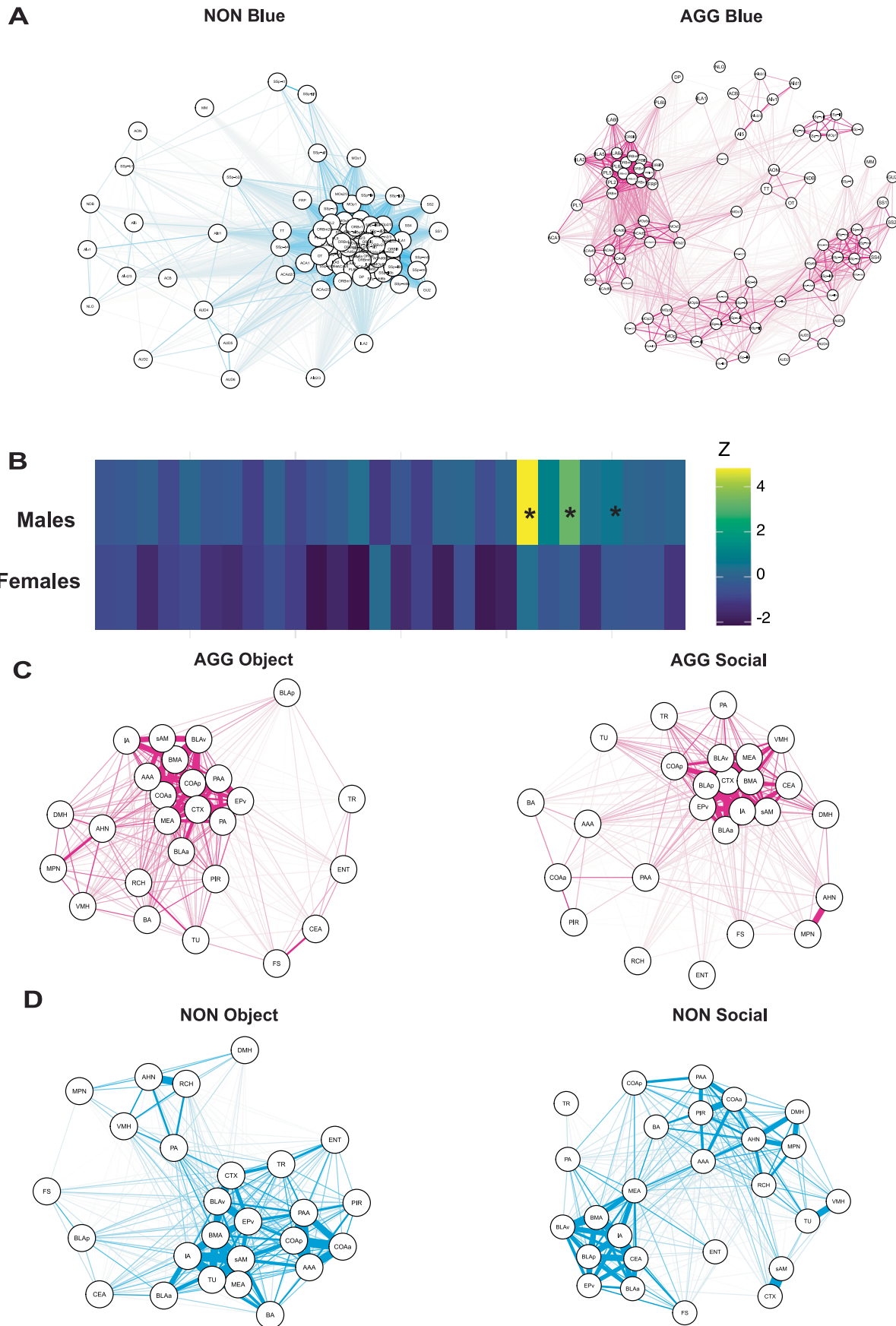
Extended Data Fig. 1 | Ethological analyses of social behaviour in AGGs and NONs. a–c, Females engage in more facial investigation than males (main effect of sex: $F_{(1,46)} = 9.725, p = 0.0031$; female AGG vs male AGG: $p = 0.0008$, female NON vs male AGG: $p = 0.0145$; Tukey's post-hoc, a), while males engaged in more flank investigation (main effect of sex: $F_{(1,46)} = 5.480, p = 0.0236$, b). There were no differences in anogenital investigation (sex x phenotype interaction:

$F_{(1,46)} = .6624, p = 0.4199$, c). d–f, Females delivered slightly more bites ($t_{(25)} = 1.808, p = 0.0827$, d) and males engaged in more wrestling behaviour ($t_{(25)} = 2.601, p = 0.0154$, e) with no differences in the number of kicks delivered ($t_{(25)} = 0.09111, p = 0.9281$, f). n = 13 male AGG, 14 female AGG, 10 male NON, 13 female NON. All data are mean \pm s.e.m.



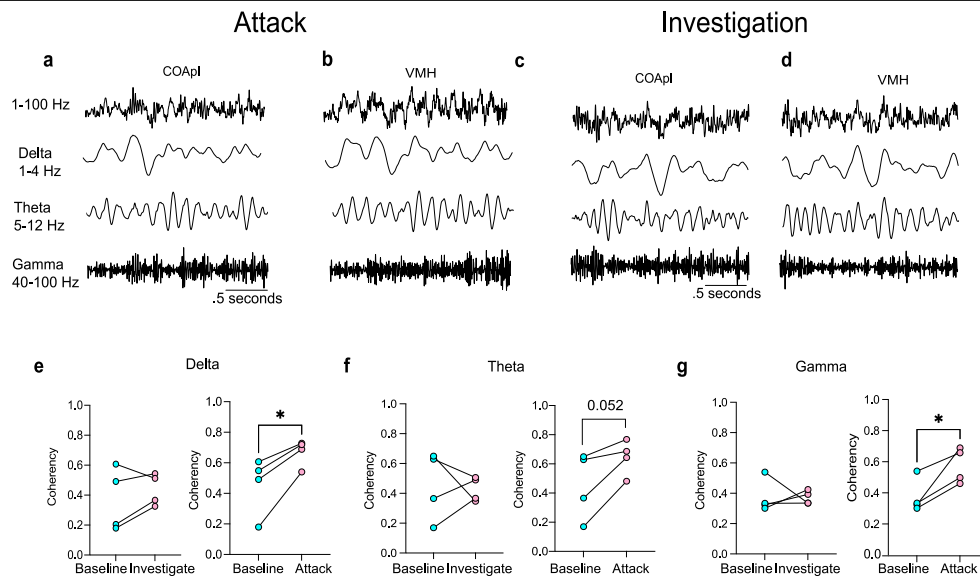
Extended Data Fig. 2 | Regional differences in FOS expression between female and male AGGs, and preservation analysis. **a–c**, Summed z-scores for density and connectivity measures in all modules. Each coloured circle corresponds to a module (**a**), z-statistics for connectivity (**b**) and density measures for each module (**c**). See Table 2 for detailed descriptions of z-statistics. **d**, Heat map of whole-brain

FOS differences between male AGG vs. NON and female AGG vs. NON. **e, f**, Top 20 regions with the largest FOS expression differences in males (**e**) and females (**f**). $n = 13$ male AGG, 14 female AGG, 10 male NON, 13 female NON. All data are mean \pm s.e.m.



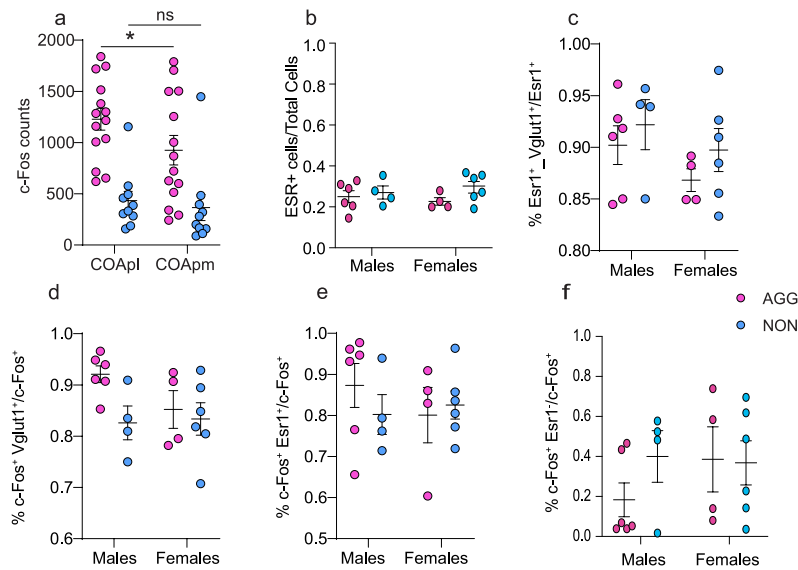
Extended Data Fig. 3 | Module preservation analyses. **a**, The blue module in the NON network (left) was not preserved in the AGG network (right). **b**, Heat map of FOS expression between male AGG vs. NON and female AGG vs. NON in the pink module. **c**, The pink module of AGGs (right) was not preserved in AGGs

who investigated a novel object. **d**, The pink module of NONs (right) was not preserved in NONs who investigated a novel object. $n = 10$ AGG object, $n = 10$ NON object, $n = 27$ AGG social, $n = 23$ NON social. All data are mean \pm s.e.m.



Extended Data Fig. 4 | Sample traces from multi-region LFPs in the COApI and VMH during attack and investigation. **a–d**, Representative traces of raw (1–100 Hz) and filtered (delta: 1–4 Hz, theta: 5–12 Hz, and gamma: 40–100 Hz) LFP signal in COApI (**a,c**), VMH (**b,d**) during attack and investigation.

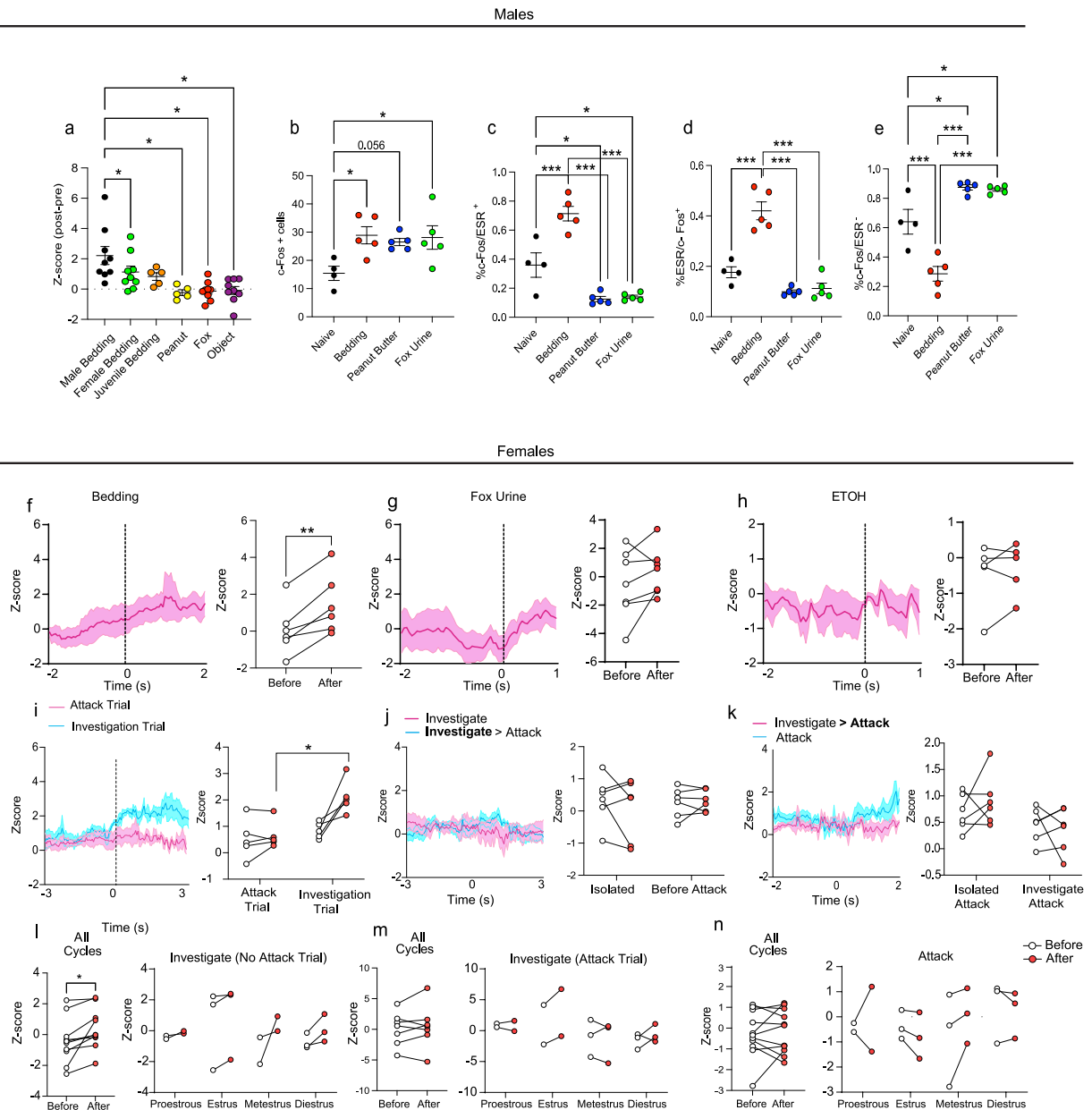
e–g, Coherence in the delta band (investigation: $t_4 = 1.121$, $p = 0.3439$; attack: $t_4 = 4.080$, $p = 0.0266$, **e**), theta band (investigation: $t_4 = 0.2230$, $p = 0.8378$; attack: $t_4 = 3.118$, $p = 0.0526$, **f**) and gamma band (investigation: $t_4 = .03658$, $p = 0.9738$; attack: $t_4 = 3.65$, $p = 0.0355$, **g**).



Extended Data Fig. 5 | Cellular phenotyping of FOS+ cells in the COAp.

a, FOS-positive cells in the COAp of males. (Phenotype: $F_{(1,22)} = 33.86, p < 0.0001$, Region: $F_{(1,22)} = 7.731, p = 0.0109$.) Post-hoc tests revealed that male AGGs had an increase of FOS-positive cells in the lateral portion of the COAp compared to the medial portion ($p = 0.014$). **b,c**, There were no group differences in the total amount of *Esr1*+ cells (sex × phenotype interaction: $F_{(1,16)} = 0.6906, p = 0.4182$, **b**), or the number of *Esr1* cells which express *Vglut1* (sex × phenotype interaction:

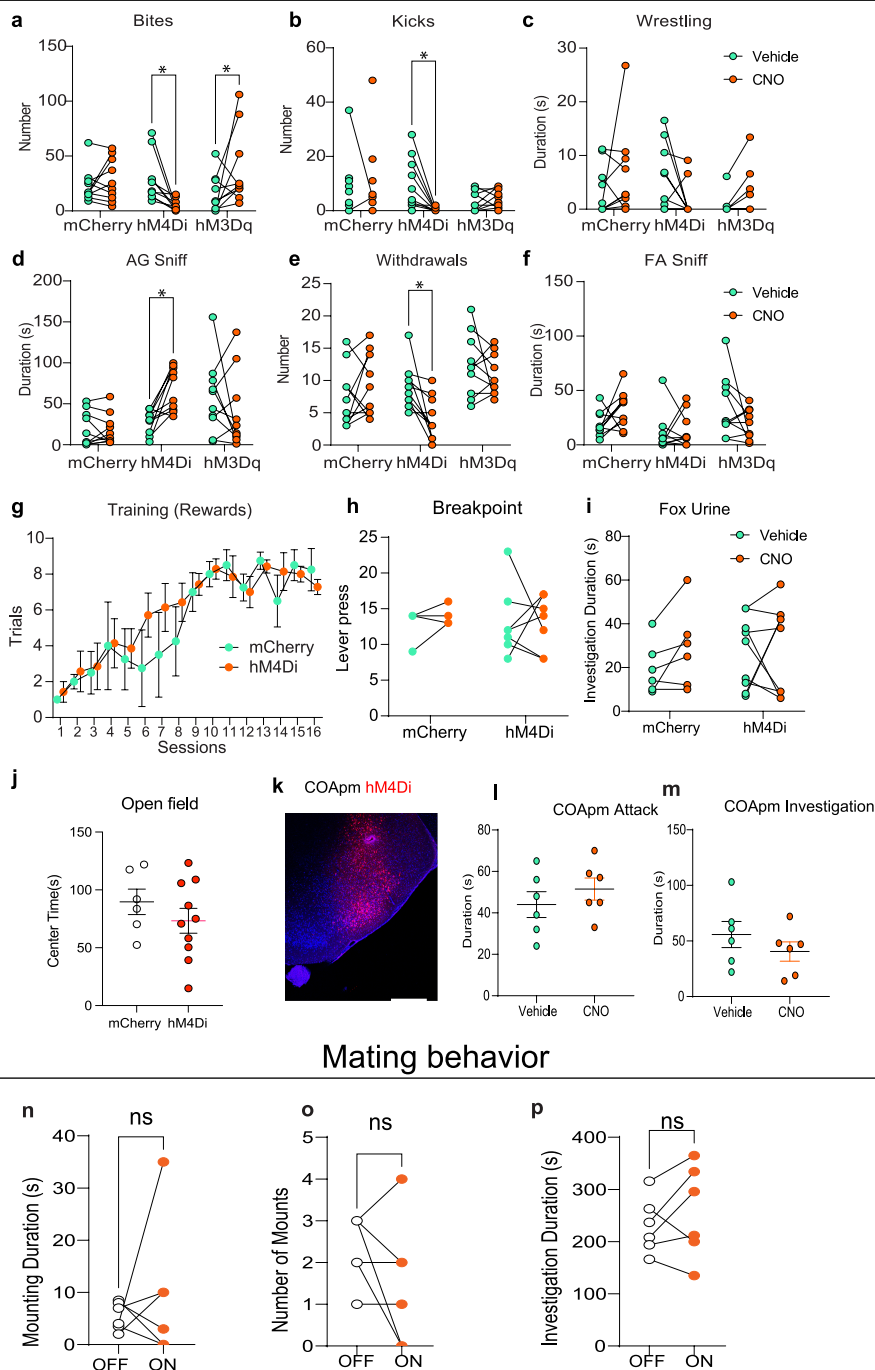
$F_{(1,16)} = 0.05229, p = 0.8220$, **c**). **d-f**, There were no group differences in the percentage of FOS+ cells which express *Vglut1* (sex × phenotype interaction: $F_{(1,16)} = 1.658, p = 0.2162$, **d**), *Esr1* (sex × phenotype interaction: $F_{(1,16)} = 0.9610, p = 0.3415$, **e**), or FOS-positive cells which did not express ESR1 (sex × phenotype interaction $F_{(1,16)} = 0.9610, p = 0.3415$, **f**). n = 6 Male AGG, 4 Female AGG, 4 Male NON, 6 Female NON. All data are mean ± s.e.m.



Extended Data Fig. 6 | Cellular phenotyping in response to odours in males and in vivo activity of COAP1^{ESR1} cells during female social behaviour.

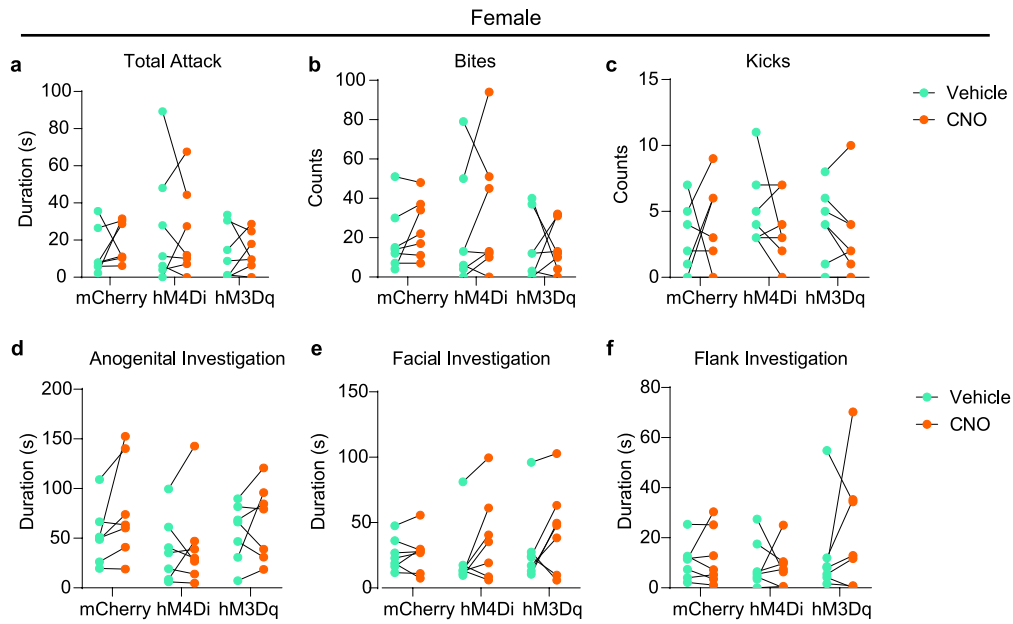
a, Post-pre differences in responses to odours ($F_{(1,587,10,14)} = 7.836, p = 0.0114$). Male bedding vs. female bedding ($p = 0.0392$), peanut odour ($p = 0.0392$), fox urine ($p = 0.0392$), or a novel object ($p = 0.0392$) $n = 9$ male bedding, $n = 9$ female bedding, $n = 5$ peanut, $n = 5$ juvenile, $n = 9$ fox urine, $n = 9$ object, Holm-Sidak post hoc. **b**, FOS expressing cells ($F_{(3,15)} = 4.112, p = 0.0258$). Naive vs. bedding ($p = 0.0152$), fox urine ($p = 0.0269$) and peanut odour ($p = 0.0558$). **c**, Percentage of FOS cells expressing ESR1 ($F_{(3,15)} = 39.02, p < 0.0001$). Bedding vs. naive ($p = 0.0004$), peanut ($p < 0.0001$) and fox urine ($p < 0.0001$). Naive vs. fox urine ($p = 0.0212$) and peanut ($p = 0.0136$). **d**, Percentage of ESR1 cells expressing FOS ($F_{(3,15)} = 39.47, p < 0.0001$), comparing responses between bedding vs. naive ($p = 0.0004$), peanut ($p < 0.0001$) and fox urine ($p < 0.0001$). **e**, FOS in ESR1⁻ cells ($F_{(3,15)} = 39.02, p < 0.0001$). **f-h**, COAP1^{ESR1} activity during the investigation

of soiled female bedding ($t_{(5)} = 5.315, p = 0.0032$, **f**), fox urine ($t_{(5)} = 1.180, p = 0.2912$, **g**), or ethanol ($t_{(4)} = 0.801, p = 0.4643$, **h**). $n = 6$ bedding, $n = 6$ fox urine, $n = 5$ ethanol. **i**, COAP1^{ESR1} activity during attack and investigation trials (interaction: $F_{(1,4)} = 6.407, p = 0.0646$, Sidak's post-hoc: $p = 0.0270, n = 5$). **j**, COAP1^{ESR1} activity during investigation bouts (interaction: $F_{(1,10)} = 1.252, p = 0.3140$, Sidak's post-hoc: $p = 0.6020$, isolated) (Sidak's post-hoc: $p = 0.9909$, before attack, $n = 6$). **k**, COAP1^{ESR1} activity during attack bouts (interaction: $F_{(1,5)} = 0.5374, p = 0.4964$, Sidak's post-hoc: $p = 0.8735$, isolated, Sidak's post-hoc: $p = 0.9881$, after investigation $n = 6$). **l-n**, COAP1^{ESR1} activity across estrous cycle. COAP1^{ESR1} activity during investigation trials ($F_{(1,6)} = 9.428, p = 0.0219$; all cycles: $t_{(9)} = 2.917, p = 0.0171, n = 10$, **l**), investigation during attack trials ($F_{(1,6)} = 1.877, p = 0.2198$, all cycles: $t_{(9)} = 1.250, p = 0.2428, n = 10$, **m**), and during aggression ($F_{(1,7)} = 0.3587, p = 0.5681$; all cycles: $t_{(10)} = 0.5035, p = 0.6255, n = 11$, **n**). All data are mean \pm s.e.m.



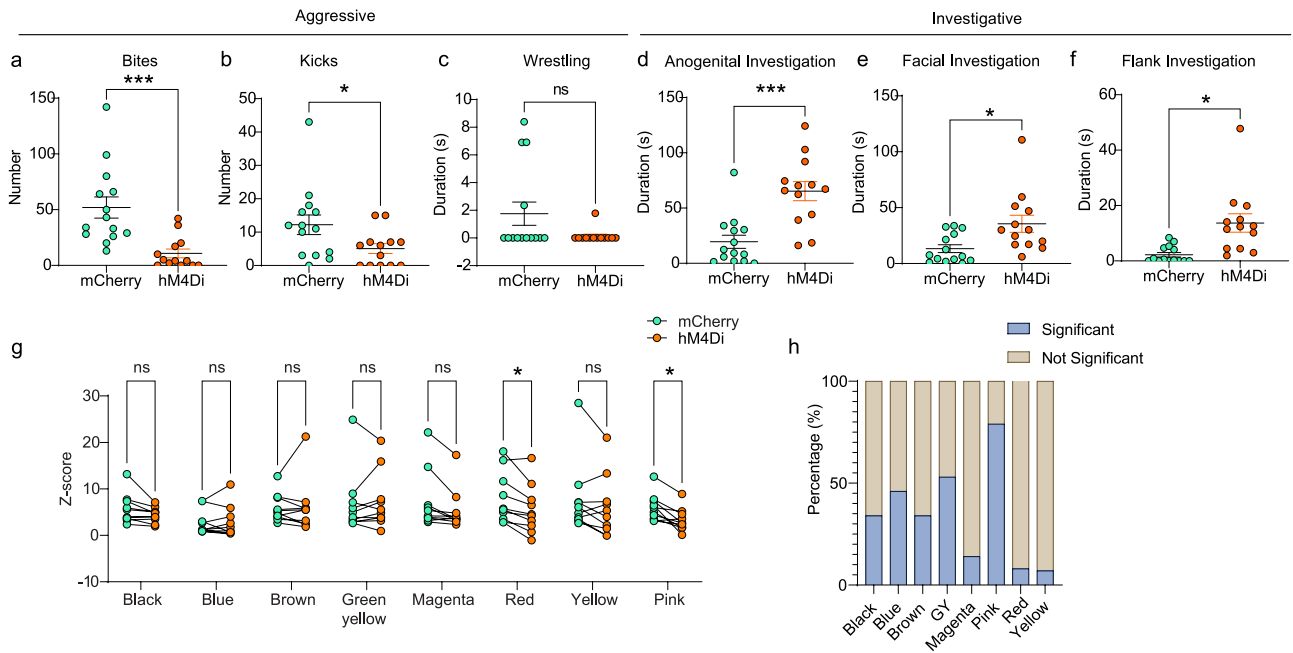
Extended Data Fig. 7 | Ethological analyses of social behaviour during RI with a male or female intruder. a-c, Number of bites (interaction: $F_{(2,27)} = 7.036$, $p = 0.0035$, **a**), kicks (interaction: $F_{(2,27)} = 3.254$, $p = 0.0542$, **b**), and wrestling (interaction: $F_{(2,27)} = 3.828$, $p = 0.0344$, **c**), following chemogenetic inhibition (bites: Sidak's post-hoc: $p = 0.0363$, kicks: Sidak's post-hoc: $p = 0.0457$, wrestling: Sidak's post-hoc: $p = 0.1729$) and excitation (bites: Sidak's post-hoc: $p = 0.0470$, kicks: Sidak's post-hoc: $p = 0.9874$, wrestling: Sidak's post-hoc: $p = 0.3511$). **d-f**, Anogenital investigation (interaction: $F_{(2,27)} = 5.634$, $p = 0.0090$, **d**), withdrawals (interaction: $F_{(2,27)} = 4.218$, $p = 0.0255$, **e**), and facial investigation (interaction: $F_{(2,27)} = 3.514$, $p = 0.0440$, **f**) following chemogenetic inhibition (anogenital investigation: Sidak's post-hoc: $p = 0.0111$, withdrawals: Sidak's post-hoc: $p = 0.0163$, facial investigation: Sidak's post-hoc: $p = 0.9903$) and excitation (anogenital investigation: Sidak's post-hoc: $p = 0.4065$, withdrawals:

Sidak's post-hoc: $p = 0.7535$, facial investigation Sidak's post-hoc: $p = 0.1537$), $n = 10$ hM4Di, 10 hM3Dq 10 mCherry. **g,h**, Acquisition of self-administration (interaction: $F_{(15,135)} = 0.7175$, $p = 0.7635$, **g**) and progressive ratio breakpoint (interaction: $F_{(1,9)} = 0.1712$, $p = 0.6887$, **h**) $n = 7$ hM4Di, 4 mCherry. **i,j**, Investigation of fox urine (interaction: $F_{(1,13)} = 0.6169$, $p = 0.4463$, $n = 9$ hM4Di, 6 mCherry, **i**) and time in centre time of an open field ($t_{14} = 1.007$, $p = 0.3308$, $n = 10$ hM4Di, 6 mCherry, **j**) following chemgenetic inhibition. **k**, Representative image of COApm infection. **l,m**, Attack ($t_{5} = 0.9657$, $p = 0.3785$, **l**) and investigation ($t_{5} = 1.127$, $p = 0.3108$, **m**) following inhibition of COApm, $n = 6$ hM4Di & mCherry. **n-p**, Mounting duration ($t_{5} = 0.7079$, $p = 0.5106$, **n**), number of mounts ($t_{5} = 1.387$, $p = 0.2242$, **o**), and investigation ($t_{5} = 1.004$, $p = 0.3616$, **p**) following inhibition of COApl. $n = 6$ NpHR. All data are mean \pm s.e.m. Scale bar: 200 μ m.



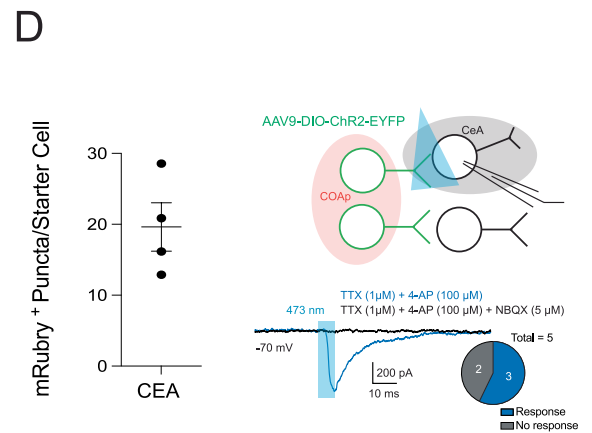
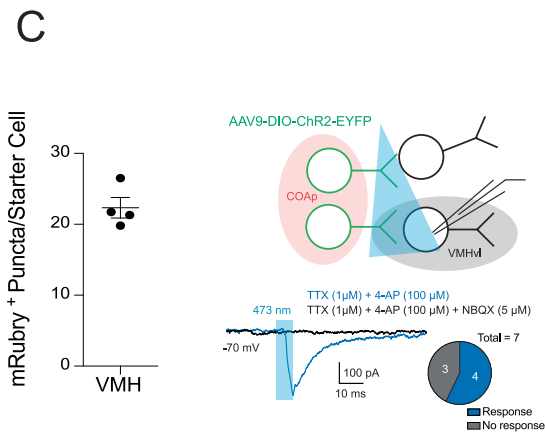
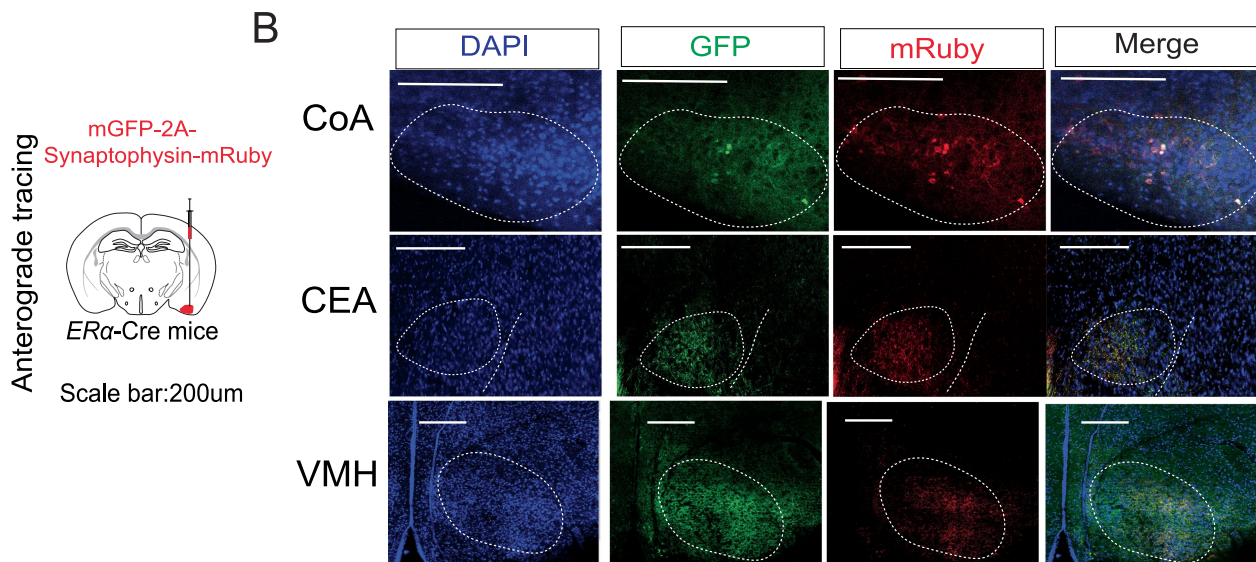
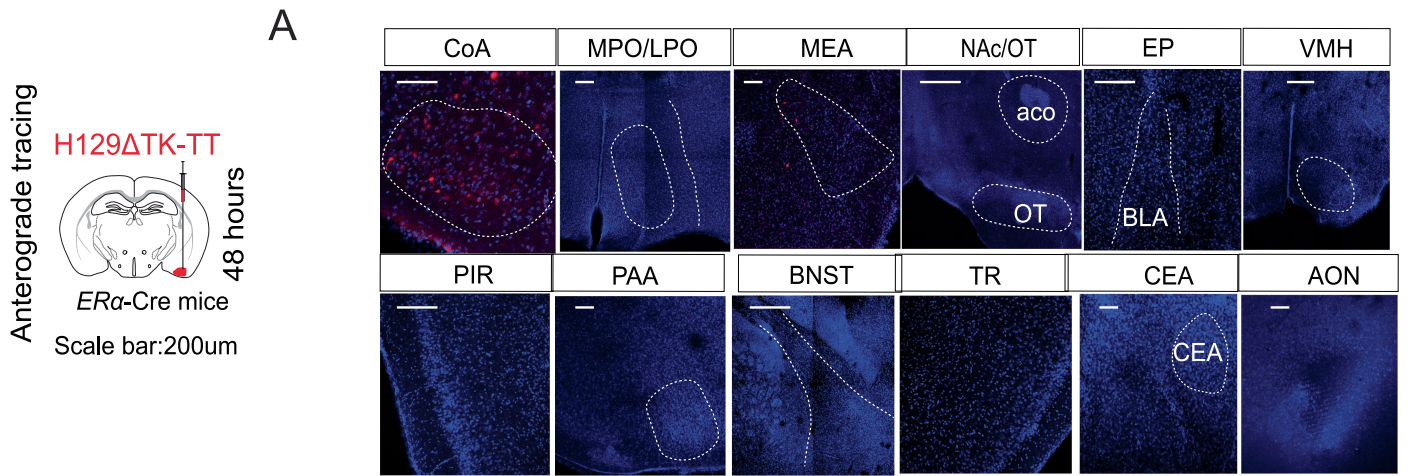
Extended Data Fig. 8 | Manipulation of COAp^{ESr1} cells has no effect on female social behaviour. **a-c**, There were no effects of inhibiting or exciting COAp^{ESr1} cells on total attack duration (virus \times drug interaction: $F_{(2,18)} = 0.2719, p = 0.7650$, **a**), bites ($F_{(2,18)} = 0.3465, p = 0.7118$, **b**) or kicks ($F_{(2,18)} = 0.9476, p = 0.4062$,

c) delivered to the intruder. **d-f**, Manipulation of COAp^{ESr1} cells did not affect anogenital (virus \times drug interaction: $F_{(2,18)} = 0.7764, p = 0.4749$, **d**), facial ($F_{(2,18)} = 1.313, p = 0.2937$, **e**), or flank ($F_{(2,18)} = 0.7432, p = 0.4896$, **f**) investigation ($n = 7$ hM4Di, 7hM3Dq & 7 mCherry). All data are mean \pm s.e.m.



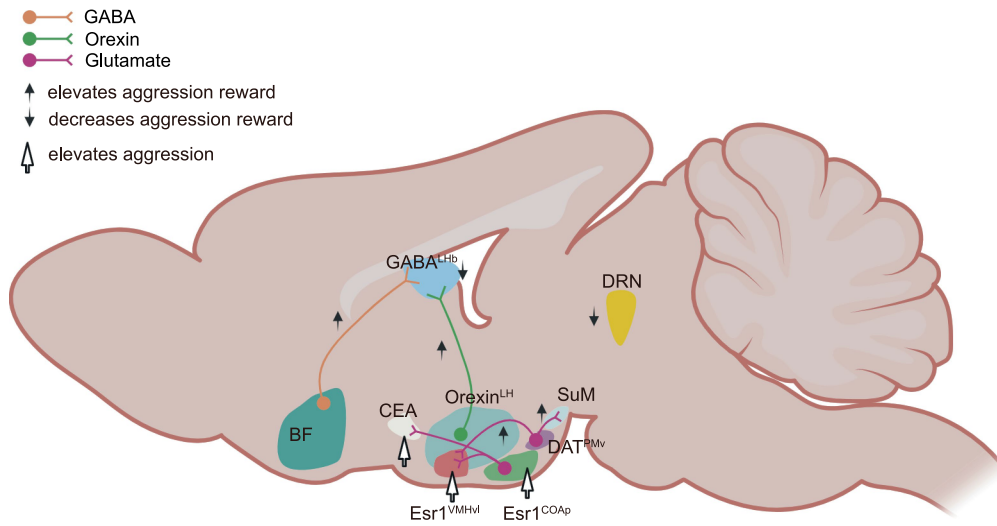
Extended Data Fig. 9 | Ethological analyses of social behaviour and preservation statistics from the DREADDiDISCO+ experiment. a–c, Inhibiting COAp^{ESR1} cells results in a reduction in bites ($t_{25} = 3.883, p = 0.0007$, **a**) and kicks ($t_{25} = 2.11, p = 0.0450$, **b**) delivered to the intruder with no effect on wrestling ($t_{25} = 1.708, p = 0.0863$, **c**) compared to the mCherry group. **d–f,** Mice injected with the hM4Di virus also displayed an increase in anogenital ($t_{25} = 4.441,$

$p = 0.0002$, **d**), facial ($t_{25} = 2.718, p = 0.0118$, **e**) and flank ($t_{25} = 3.496, p = 0.0018$, **f**) investigation $n = 13$ hM4Di, 14 mCherry. **g,** In addition to the pink module, inhibiting the COAp alters the preservation of the red module ($t_0 = 3.600, q = 0.022980$). **h,** The pink module had the highest percentage of regions (85%) which showed a decrease in FOS. All data are mean \pm s.e.m.



Extended Data Fig. 10 | Verification of monosynaptic connectivity between the COAp and the VMH and CEA. **a**, HSV-1 trans-synaptic anterograde tracing after 48 h. There were no downstream labelled cells in the VMH or CEA. Scale bar, 100 μm. **b**, Anterograde tracing with AAV-hSyn-FLEX-mGFP-2A-Synaptophysin-mRuby confirmed monosynaptic connectivity between ESRI⁺ cells in the COAp and the VMH and CEA. Scale bar: 200 μm. **c**, Quantification of mRuby⁺ puncta (left) and ChR2-assisted circuit mapping of COAp^{ESRI}→VMH pathway showing monosynaptic (with TTX) glutamatergic (NBQX) excitatory

(Cs-based internal, clamped at -70 mV) connections in 4/7 VMH cells. **d**, Quantification of mRuby⁺ puncta (left) and ChR2-assisted circuit mapping of COAp^{ESRI}→CEA pathway showing monosynaptic (with TTX) glutamatergic (NBQX) excitatory connections (Cs-based internal, clamped at -70 mV) in 3/4 CEA neurons. n = 3 mice for ChR2-assisted circuit mapping and N = 4 for anterograde tracing. The illustrations were created with BioRender. All data are mean ± s.e.m.



Extended Data Fig. 11 | Schematic of brain regions involved in aggression and aggression reward. Activity of the COAp and its outputs to the VMH and CEA enhance aggressive social behaviour. By contrast, the activity of the basal forebrain (BF) and ventral preammillary nucleus (PMv) enhance the rewarding

properties of aggression, whereas the lateral habenula (LHb) and dorsal raphe nucleus (DRN) decrease the rewarding properties of aggression. The illustration was created with BioRender.

Reporting Summary

Nature Portfolio wishes to improve the reproducibility of the work that we publish. This form provides structure for consistency and transparency in reporting. For further information on Nature Portfolio policies, see our [Editorial Policies](#) and the [Editorial Policy Checklist](#).

Statistics

For all statistical analyses, confirm that the following items are present in the figure legend, table legend, main text, or Methods section.

- | | |
|-------------------------------------|---|
| n/a | Confirmed |
| <input type="checkbox"/> | <input checked="" type="checkbox"/> The exact sample size (n) for each experimental group/condition, given as a discrete number and unit of measurement |
| <input type="checkbox"/> | <input checked="" type="checkbox"/> A statement on whether measurements were taken from distinct samples or whether the same sample was measured repeatedly |
| <input type="checkbox"/> | <input checked="" type="checkbox"/> The statistical test(s) used AND whether they are one- or two-sided
<i>Only common tests should be described solely by name; describe more complex techniques in the Methods section.</i> |
| <input checked="" type="checkbox"/> | <input type="checkbox"/> A description of all covariates tested |
| <input type="checkbox"/> | <input checked="" type="checkbox"/> A description of any assumptions or corrections, such as tests of normality and adjustment for multiple comparisons |
| <input checked="" type="checkbox"/> | <input type="checkbox"/> A full description of the statistical parameters including central tendency (e.g. means) or other basic estimates (e.g. regression coefficient) AND variation (e.g. standard deviation) or associated estimates of uncertainty (e.g. confidence intervals) |
| <input type="checkbox"/> | <input checked="" type="checkbox"/> For null hypothesis testing, the test statistic (e.g. F , t , r) with confidence intervals, effect sizes, degrees of freedom and P value noted
<i>Give P values as exact values whenever suitable.</i> |
| <input checked="" type="checkbox"/> | <input type="checkbox"/> For Bayesian analysis, information on the choice of priors and Markov chain Monte Carlo settings |
| <input checked="" type="checkbox"/> | <input type="checkbox"/> For hierarchical and complex designs, identification of the appropriate level for tests and full reporting of outcomes |
| <input type="checkbox"/> | <input checked="" type="checkbox"/> Estimates of effect sizes (e.g. Cohen's d , Pearson's r), indicating how they were calculated |

Our web collection on [statistics for biologists](#) contains articles on many of the points above.

Software and code

Policy information about [availability of computer code](#)

Data collection Fiber photometry data was acquired with open source Bonsai software 2.4.0 and custom Neurophotometrics (Neurophotometrics, Ltd) hardware. Cleared brain imaging was done on lightsheet microscope (LaVision).

Data analysis Analysis of fiber photometry data was performed with R. Histological data was analyzed using Fiji. Cleared brain data was analyzed by ClearMap (python).

For manuscripts utilizing custom algorithms or software that are central to the research but not yet described in published literature, software must be made available to editors and reviewers. We strongly encourage code deposition in a community repository (e.g. GitHub). See the Nature Portfolio [guidelines for submitting code & software](#) for further information.

Data

Policy information about [availability of data](#)

All manuscripts must include a [data availability statement](#). This statement should provide the following information, where applicable:

- Accession codes, unique identifiers, or web links for publicly available datasets
- A description of any restrictions on data availability
- For clinical datasets or third party data, please ensure that the statement adheres to our [policy](#)

All raw data for animal behaviours, fiber photometry, in vivo LFP recordings, and ISH are available as Source data files.

Research involving human participants, their data, or biological material

Policy information about studies with [human participants or human data](#). See also policy information about [sex, gender \(identity/presentation\), and sexual orientation](#) and [race, ethnicity and racism](#).

Reporting on sex and gender

Use the terms *sex* (biological attribute) and *gender* (shaped by social and cultural circumstances) carefully in order to avoid confusing both terms. Indicate if findings apply to only one sex or gender; describe whether sex and gender were considered in study design; whether sex and/or gender was determined based on self-reporting or assigned and methods used. Provide in the source data disaggregated sex and gender data, where this information has been collected, and if consent has been obtained for sharing of individual-level data; provide overall numbers in this Reporting Summary. Please state if this information has not been collected. Report sex- and gender-based analyses where performed, justify reasons for lack of sex- and gender-based analysis.

Reporting on race, ethnicity, or other socially relevant groupings

Please specify the socially constructed or socially relevant categorization variable(s) used in your manuscript and explain why they were used. Please note that such variables should not be used as proxies for other socially constructed/relevant variables (for example, race or ethnicity should not be used as a proxy for socioeconomic status). Provide clear definitions of the relevant terms used, how they were provided (by the participants/respondents, the researchers, or third parties), and the method(s) used to classify people into the different categories (e.g. self-report, census or administrative data, social media data, etc.) Please provide details about how you controlled for confounding variables in your analyses.

Population characteristics

Describe the covariate-relevant population characteristics of the human research participants (e.g. age, genotypic information, past and current diagnosis and treatment categories). If you filled out the behavioural & social sciences study design questions and have nothing to add here, write "See above."

Recruitment

Describe how participants were recruited. Outline any potential self-selection bias or other biases that may be present and how these are likely to impact results.

Ethics oversight

Identify the organization(s) that approved the study protocol.

Note that full information on the approval of the study protocol must also be provided in the manuscript.

Field-specific reporting

Please select the one below that is the best fit for your research. If you are not sure, read the appropriate sections before making your selection.

Life sciences Behavioural & social sciences Ecological, evolutionary & environmental sciences

For a reference copy of the document with all sections, see [nature.com/documents/nr-reporting-summary-flat.pdf](https://www.nature.com/documents/nr-reporting-summary-flat.pdf)

Life sciences study design

All studies must disclose on these points even when the disclosure is negative.

Sample size

Sample sizes are based on previous papers.

Data exclusions

One animal was excluded from the ISH analysis (Figure S6B-E, naive group) based on Grubb's test. In experiments requiring viral infection of a specific brain region, mice were excluded from behavioral analysis if the virus was found to be mis-targeted or not expressed according to pre-determined anatomical criteria. No data was excluded for other reasons.

Replication

Data was collected using biological replicates (e.g. multiple brain slices per animal analyzed for in-situ hybridization). Data from DREADD and optogenetic manipulations are based on 2 independent cohorts. All attempts at replication were successful.

Randomization

For assignment to viral groups, mice were screened for aggressive behavior and randomly assigned to groups.

Blinding

While experimenters were not blind to group allocation for data collection, analyses were performed blind to experimental conditions (Behavioral scoring from videos, fiber photometry analysis, quantification of in-situ hybridization results).

Reporting for specific materials, systems and methods

We require information from authors about some types of materials, experimental systems and methods used in many studies. Here, indicate whether each material, system or method listed is relevant to your study. If you are not sure if a list item applies to your research, read the appropriate section before selecting a response.

Materials & experimental systems

Methods

- n/a Involved in the study
- Antibodies
- Eukaryotic cell lines
- Palaeontology and archaeology
- Animals and other organisms
- Clinical data
- Dual use research of concern
- Plants

- n/a Involved in the study
- ChIP-seq
- Flow cytometry
- MRI-based neuroimaging

Animals and other research organisms

Policy information about [studies involving animals](#); [ARRIVE guidelines](#) recommended for reporting animal research, and [Sex and Gender in Research](#)

Laboratory animals	SW: Obtained from Charles River labs (male, 4-6 months of age, Strain Code 024). ER α -Cre: B6N.129S6(Cg)-Esr1tm1.1(cre)And/J, Obtained from Jackson Laboratory (male, 10 weeks of age, Stock No: 017911), were crossed with SW wild-type mice for one generation to generate ER α -Cre/SW F1 hybrids. Male F1 hybrids 3-4 months of age were used for experiments. Female F1 hybrids were co-housed with F1 males prior to testing.
Wild animals	N/A
Reporting on sex	Findings from fiber photometry and DREADD experiments were only found in one sex (Males). Data from females are in extended figures.
Field-collected samples	N/A
Ethics oversight	Mouse experiments were performed in accordance with the National Institutes of Health Guide for Care and Use of Laboratory Animals and the Icahn School of Medicine at Mount Sinai Institutional Animal Care and Use Committee.

Note that full information on the approval of the study protocol must also be provided in the manuscript.

Plants

Seed stocks	<i>Report on the source of all seed stocks or other plant material used. If applicable, state the seed stock centre and catalogue number. If plant specimens were collected from the field, describe the collection location, date and sampling procedures.</i>
Novel plant genotypes	<i>Describe the methods by which all novel plant genotypes were produced. This includes those generated by transgenic approaches, gene editing, chemical/radiation-based mutagenesis and hybridization. For transgenic lines, describe the transformation method, the number of independent lines analyzed and the generation upon which experiments were performed. For gene-edited lines, describe the editor used, the endogenous sequence targeted for editing, the targeting guide RNA sequence (if applicable) and how the editor was applied.</i>
Authentication	<i>Describe any authentication procedures for each seed-stock-used or novel genotype generated. Describe any experiments used to assess the effect of a mutation and, where applicable, how potential secondary effects (e.g. second site T-DNA insertions, mosaicism, off-target gene editing) were examined.</i>